Title: ULK1 Inhibition Promotes Oxidative Stress-Induced Differentiation and Sensitizes Leukaemic Stem Cells to Targeted Therapy

Authors: Angela Ianniciello[1], Martha M. Zarou[1†], Kevin M. Rattigan[1†], Mary Scott[1], Amy Dawson[1], Karen Dunn[2], Zuzana Brabcova[1], Eric R. Kalkman[1], Colin Nixon[3], Alison M. Michie[2], Mhairi Copland[2], David Vetrie[1], Martin Ambler[4], Barbara Saxty[4] and G. Vignir Helgason[1*]

Affiliations:

[1]Wolfson Wohl Cancer Research Centre, Institute of Cancer Sciences, University of Glasgow, Glasgow, G61 1QH, UK

[2]Paul O'Gorman Leukaemia Research Centre, Institute of Cancer Sciences, University of Glasgow, Glasgow, G12 0ZD, UK

[3]Cancer Research UK Beatson Institute, Glasgow, G61 1BD, UK

[4]LifeArc, Accelerator Building, Open Innovation Campus, Stevenage, SG1 2FX, UK

[†]These authors contributed equally to this work

[*]Corresponding author: G. Vignir Helgason, Wolfson Wohl Cancer Research Centre, Institute of Cancer Sciences, University of Glasgow, G61 1QH, UK Vignir.Helgason@glasgow.ac.uk

One Sentence Summary: ULK1 inhibition increases the sensitivity of leukaemia stem cells to TKI therapy by modulating energy and redox balance.

Abstract: Inhibition of autophagy has been proposed as a potential therapy for individuals with cancer. However, current lysosomotropic autophagy inhibitors have demonstrated limited efficacy in clinical trials. Therefore, validation of novel specific autophagy inhibitors using robust pre-clinical models is critical. In chronic myeloid leukaemia (CML), minimal residual disease is maintained by persistent leukaemic stem cells (LSCs), which drive tyrosine kinase inhibitor (TKI) resistance and patient relapse. Here we show that deletion of autophagy-inducing kinase ULK1 reduces growth of cell line and patient-derived xenografted CML cells in mouse models. Using primitive cells, isolated from individuals with CML, we demonstrate that pharmacological inhibition of ULK1 selectively targets CML LSCs ex vivo and in vivo, when combined with TKI treatment. The enhanced TKI sensitivity following ULK1-mediated autophagy inhibition is driven by increased mitochondrial respiration, loss of quiescence, and points to oxidative stress-induced differentiation of CML LSCs, proposing an alternative strategy for treating patients with CML.

INTRODUCTION

Macroautophagy (hereafter referred to as autophagy) is an evolutionarily conserved, lysosome-dependent, catabolic process that maintains cellular energy amounts during starvation or metabolic stress. Whereas non-selective autophagy involves uptake of cytoplasmic cargo into forming autophagosomes, selective autophagy is accountable for specifically removing redundant components from cells such as protein aggregates and organelles, including superfluous mitochondria (mitophagy) (*1*). Numerous pre-clinical studies have demonstrated that autophagy plays a predominantly cytoprotective role in the context of cancer, highlighting the potential benefit of combining autophagy inhibition with current anti-cancer therapies (*2*). Whereas the lysosomotropic agent hydroxychloroquine (HCQ) inhibits autophagy in pre-clinical cancer models, a major drawback in the field is the lack of potency and efficacy of HCQ as an autophagy inhibitor in clinical trials (*3-6*). These phase I/II studies have demonstrated that maximal achievable doses of HCQ (up to 1200mg/day) do not consistently inhibit autophagy in cancer patients, driving the development of more potent compounds, with similar chemical and lysosomotropic properties as HCQ (*7*), or more selective autophagy inhibitors that target proteins required for autophagy initiation (*8-12*).

The nutrient-sensing mechanistic target of rapamycin complex 1 (mTORC1) is a serine/threonine kinase complex that inhibits autophagy through phosphorylation of downstream autophagy related (ATG) proteins (*13-16*). Accordingly, inhibition of mTORC1 leads to activation of the unc-51-like autophagy activating kinase 1 (ULK1) complex, consisting of ULK1 itself, autophagy related 13 (ATG13), focal adhesion kinase family interacting protein of 200 kDa (FIP200) and autophagy related 101 (ATG101). Autophagy regulation is also mediated by energy-sensing AMP-activated protein kinase (AMPK), which is activated in response to reduced intracellular ATP

concentrations, caused by nutrient deprivation or inhibition of mitochondrial function. Activated AMPK mediates its effect by direct phosphorylation of ULK1 (*15-17*), leading to ULK1 activation and phosphorylation of its downstream targets, including ATG13 (*18*). This triggers the initiation of the autophagy cascade, leading to the recruitment of an ubiquitin-like conjugation system and the conjugation of microtubule-associated protein 1 light chain 3 (LC3) to phosphatidylethanolamine (PE) on the phagophore (the precursors to autophagosomes), followed by autophagosome lysosome fusion (*19*). Activation of the ULK1 complex is one of the first critical steps in the autophagy process, and ULK1 is a druggable serine/threonine kinase (*10-12*), therefore, ULK1 represents an attractive target for pharmacological inhibition of autophagy (*2, 19*).

Chronic myeloid leukaemia (CML) is a stem cell driven myeloproliferative disorder, caused by t(9;22)(q34;q11) chromosomal translocation in a single haematopoietic stem cell (HSC). The defective chromosome 22, also known as the Philadelphia chromosome, carries the chimeric *BCR-ABL* oncogene, which codes for a fusion oncoprotein with constitutive tyrosine kinase activity. The introduction of imatinib and other second and third generation tyrosine kinase inhibitors (TKIs) has transformed the clinical management of CML (*20, 21*) and represents a paradigm for targeted therapy in cancer with the potential for cure (*22*). However, up to half of patients with stable deep molecular response (DMR) that qualify for TKI discontinuation trials relapse within 12 months (*23*). Hence, only 10-15% of CML patients achieve sustained treatment-free remission (TFR) (*24*). In addition, the vast majority of the patients requires life-long TKI treatment, associated with chronic side effects, including chronic anaemia, which in turn has been linked to less favourable treatment responses (*25, 26*). Furthermore, 20-30% of CML patients develop resistance to TKIs or progress to lethal blast phase (BP) with very limited therapeutic options (*24*).

It has been demonstrated that leukaemic stem cells (LSCs) are inherently insensitive to TKI treatment (*27, 28*). Indeed, LSCs are detectable in virtually all TKI-treated CML patients, including those who achieve DMR (*29*). We have previously demonstrated that TKI treatment induces protective autophagy in CML LSCs ex vivo (*30*) and in vivo (*31*). However, chloroquine and imatinib combination to eliminate stem cells (CHOICES), a phase II clinical trial where imatinib combined with HCQ-mediated autophagy inhibition was tested in chronic phase (CP)-CML patients, showed limited potency of HCQ and only a modest reduction in minimal residual disease (MRD) as assessed by qRT-PCR for *BCR-ABL* (*6*). These results highlight the need for developing and testing specific autophagy inhibitors in order to achieve frequent and deeper molecular responses for patients with CML, enabling more patients to attempt and maintain TFR.

Here we present our findings regarding the mechanism through which ULK1 regulates TKI-induced autophagy, central carbon metabolism, differentiation, and drug sensitivity of primitive leukaemia cells. Using patient-derived CML cells, and autophagy-deficient cell lines, we demonstrate that TKI treatment leads to AMPK and ULK1 activation and subsequently, an increase in ULK1-dependent autophagy flux. Genetic deletion of ULK1, or treatment with an ULK1 kinase inhibitor, MRT403, blocked TKI-induced autophagy and promoted a metabolic shift from glycolysis to mitochondrial respiration. This led to increased oxidative stress and reactive oxygen species (ROS)-dependent differentiation. Finally, we demonstrated that combined BCR-ABL and ULK1 inhibition restored a normal ratio of immature myeloid and erythroid cells in the bone marrow (BM) and targeted therapy-resistant CML LSCs in both transgenic and patient-derived xenograft (PDX) CML models, further supporting the concept that specific autophagy inhibition may enhance anti-cancer therapy.

RESULTS

ULK1 is a Key Mediator of TKI-Induced Autophagy

mTORC1 and AMPK integrate energy signals to maintain cellular homeostasis by balancing anabolic and catabolic processes, including autophagy. To assess whether TKI-mediated BCR-ABL inhibition affected AMPK and mTORC1 activity in primary CML cells, stem/progenitor ($CD34^+$) cells were isolated from four individuals with CP-CML at diagnosis (table S1) and treated with the TKI nilotinib in serum-free medium supplemented with low concentrations of human growth factors (*32*). As expected, nilotinib treatment inhibited BCR-ABL kinase activity, measured by decreased phosphorylation of CrkL (Fig. 1A and fig S1A). Furthermore, nilotinib decreased ULK1 phosphorylation on serine 757 and increased phosphorylation on serine 555 suggesting inhibition of mTORC1 (*15*), and activation of AMPK (*17*), respectively (Fig. 1A and fig S1, B and C). Time-course experiment (n=5) demonstrated that nilotinib treatment rapidly inhibited mTORC1 activity, measured by decreased phosphorylation of ribosomal protein S6 (RPS6), and led to gradual time-dependent AMPK activation, demonstrated by an increase in phosphorylation on the conserved threonine 172 (Fig. 1B-C and fig. S1D-K). The increased phosphorylation of ATG13, confirmed activation of the autophagy-inducing ULK1 complex (*13, 14, 18*). Although patient variability in LC3B-II concentrations was observed, the time-dependent reduction in the autophagy cargo receptor sequestosome 1 (SQSTM1/p62) indicated consistent induction of autophagy flux following nilotinib-mediated BCR-ABL inhibition. In addition to the increase in TKI-mediated autophagy, we observed an increase in mRNA transcript expression of key autophagy related genes, including members of the ULK1 complex (fig. S1L). We therefore hypothesised that ULK1 is a central energy-sensing node and required for TKI-induced autophagy in CML cells (fig. S1M). We next employed KCL22 cells, human BP-CML cell line, and CRISPR-Cas9 technology to test whether specific inhibition of ULK1 affected autophagy flux in CML cells.

Consistent with $CD34^+$ CML cells, ULK1 activity and autophagy flux was visible in nilotinib treatment control cells (Fig. 1D and fig. S1N). ULK1 knockout (KO) in KCL22 cells prevented ATG13 phosphorylation and TKI-induced autophagy in multiclonal and single cell KO clones. Similar results were obtained with imatinib treatment of KCL22 cells, confirming a BCR-ABL mediated effect (Fig. 1D). Colony forming cell (CFC) assays demonstrated increased sensitivity of ULK1-deficient cells to BCR-ABL inhibition (fig. S1O).

KCL22 cells form extramedullary tumours when transplanted via tail vein injection into immunocompromised mice and are suitable for target assessment studies. To test whether ULK1 deletion affects tumour formation in vivo, KCL22 cells were labelled with luciferase and transplanted by tail vain injection into non-irradiated immunocompromised mice. Mice were then left untreated or treated for 4 weeks with imatinib (50mg/kg BID), front-line treatment for CML patients, and monitored weekly by luciferase bio-imaging. This revealed a decrease in bioluminescence in mice transplanted with ULK1-deficient cells, compared to mice receiving control cells (Fig. 1E), and a significant ($P = 0.0025$) reduction in number of tumours at week 4 (Fig. 1F). Notably, imatinib treatment significantly ($P = 0.008$) reduced tumour burden in mice transplanted with ULK1-KO cells, when compared with imatinib-treated mice xenografted with autophagy-competent cells (Fig. 1, E and F). In a separate transplant experiment, although imatinib treatment had no effect on overall survival of mice transplanted with ULK1 expressing cells, consistent with the lack of efficacy of imatinib in the blast phase of the disease, it significantly ($P = 0.0033$) prolonged survival of ULK1-KO xenografted mice (Fig. 1G). These results suggest a specific role for ULK1 in drug resistance and encouraged us to examine further the consequence of pharmacological or genetic ULK1 inhibition on autophagy and energy homeostasis in CML cells.

Inhibition of ULK1 Induces Oxidative Stress by Promoting a Metabolic Shift from Glycolysis to Oxidative Mitochondrial Metabolism

We previously developed MRT68921, which potently inhibits ULK1 in vitro and blocks mTORC1-mediated autophagy (*10*). However, similar to other available ULK1 inhibitors (*11, 12*), MRT68921 displayed only modest specificity, which results in undesired ULK1-independent cytotoxic effects. We have subsequently developed MRT403 with comparable potency (IC50 ULK1 1.6nM). Improved kinase selectivity was first illustrated for MRT403 in a single point screen against a panel of 80 kinases (fig. S2A). The screen was conducted at a high concentration (1μM) at which ULK1 and ULK2 are inhibited greater than 90% for both compounds. No other kinases were inhibited to this level by MRT403. In contrast MRT68921 inhibited 11 other kinases, at greater than 90% inhibition and these included TANK binding kinase 1 (TBK1), AMPK and AMPK-related enzymes as previously reported (10), which could impact on autophagy. In vitro selectivity greater than 30-fold for ULK1 versus these targets for MRT403 was confirmed by potency measurements (table S2) and would suggest interfering off-target cellular activity would be unlikely. Western blotting showed confirmed ULK1 inhibition without affecting BCR-ABL activity (fig. S2B). To assess autophagy cargo degradation in CML cells, we generated a K562 cell line stably expressing YFP-Parkin, enabling precise measurements of the rate of autophagy in response to agents that modulate autophagy flux (*33, 34*). Using this system, autophagy-dependent removal of mitochondria, also known as mitophagy, is induced. Mitophagy was measured by reduction in electron transport chain (ETC) proteins, following treatment with the ETC complex III inhibitor antimycin A and the ATP synthase inhibitor oligomycin in K562 YPF-Parkin cells (fig. S2C). Basal and stress-induced mitophagy was not apparent in clonal ULK1-deficient cells or when autophagy related 7 (ATG7), an enzyme required for LC3-PE conjugation (*35*), was

deleted (fig. S2D). The increase in mitochondria in ULK1 and ATG7 KO cells was confirmed in live cells using green-fluorescent mitochondrial stain (fig. S2E). We next measured the effect of MRT403 treatment on autophagy inhibition. Treatment of YFP-Parkin expressing CML cells with increasing concentrations of MRT403 inhibited autophagic degradation of ETC complex components in a concentration-dependent manner, with complete inhibition of autophagy achieved at 3μM (fig. S2, F and G). Similar results were obtained using MRT68921 (fig. S2, H and I). HCQ-mediated autophagy inhibition required 10μM HCQ for complete inhibition, although inhibition of basal mitophagy was evident at 3μM HCQ (fig. S2, J and K). This prompted us to investigate whether pharmacological ULK1 inhibition affected basal autophagy in primary patient-derived cells. Treatment of $CD34^+$ CML cells (n=5) with 3μM MRT403 affected LC3B-II levels, in line with previous studies suggesting accumulation of stalled early autophagosomal structures (*10, 36*). In addition, ETC complex concentrations were consistently increased, suggesting impairment in autophagy-dependent mitochondrial clearance (Fig. 2, A and B). Similar results were obtained by flow cytometry following pharmacological autophagy inhibition in live cells (fig. S2L).

The acute increase of mitochondria in patient-derived CML cells resulted in an overall increase in basal mitochondrial respiration and maximal respiratory capacity, measured by an increase in basal cellular oxygen consumption rate (OCR) or following treatment with the mitochondrial uncoupler FCCP (n=4; Fig. 2C). Similar results were obtained in MRT68921 treated KCL22 cells (fig. S2M). An increase in mitochondrial respiration was also apparent in ULK1 and ATG7-deficient cells (Fig. 2D). MRT403 treatment did not have any additional effect in autophagy-deficient cells, confirming that the increase in OCR following pharmacological ULK1 inhibition was dependent on inhibition of the autophagy process.

Since electron leakage in the ETC is the principal source of ROS, we hypothesized that increased mitochondrial respiration in autophagy inhibited CML cells would lead to increased oxidative stress. To address this, patient-derived $CD34^+$ CML cells (n=5) were treated with MRT403, and mitochondrial superoxide was measured. This revealed an increase in mitochondrial ROS following ULK1 inhibition, which was completely abrogated by the addition of the antioxidant N-acetyl-L-cysteine (NAC) (Fig. 2E). Similar results were obtained in ULK1-deficient cells (Fig. 2F), and following treatment with MRT68921, whereas the effect of 3μM HCQ on mitochondrial ROS were not significantly different compared with untreated cells ($p > 0.05$; fig. S2N).

Consistently, ULK1 has been shown to maintain redox homeostasis following nutritional stress by direct phosphorylation of key glycolytic enzymes (*37*). This autophagy independent effect sustains glycolysis and the pentose phosphate pathway (PPP), leading to increased NADPH production and protection from oxidative stress. We therefore tested whether ULK1 inhibition affects glycolysis in vitro. Treatment with MRT403 significantly ($P = 0.010$) reduced glycolysis in $CD34^+$ CML cells (n=5; Fig. 2G), measured by extracellular acidification rate (ECAR), which was similar to the effect observed following treatment with MRT68921 in these cells (n=3; fig. S3A). Whereas decreased glycolysis was also observed in ULK1-deficient cells, this was not the case in ATG7-deficient cells, suggesting an ULK1-dependent, autophagy-independent effect (Fig. 2H). Concurrently, treatment with MRT403 reduced ECAR in ATG7-deficient cells but had no additive effect in ULK1-KO cells, confirming an ULK1-dependent effect. Furthermore, together with reduced glycolysis, $CD34^+$ CML cells exhibited a reduced $NADPH/NADP^+$ ratio following MRT403 treatment, suggesting a decrease in carbon flux to the PPP (Fig. 2I). An increase in total cellular ROS amounts following ULK1 inhibition in $CD34^+$ cells was also observed, indicating increased oxidative stress (fig. S3B), although without a significant increase in apoptosis or DNA

damage (fig. S3, C and D). Similarly, no increase in DNA damage was observed following pharmacological or genetic ULK1 inhibition in CML cells (fig. S3, E and F).

Inhibition of ULK1 Promotes Loss of Quiescence and ROS-Dependent Differentiation Ex Vivo

Increased mitochondrial activity and oxidative stress have been associated with loss of quiescence and enhanced differentiation of HSCs (*38, 39*). We therefore hypothesised that ULK1 inhibition would drive loss of quiescence and reduce the number of phenotypic CML LSCs ex vivo. To address this, we treated patient-derived $CD34^+$ CML cells (n=4) with MRT403 and performed cell cycle analysis using the proliferation marker Ki67 and propidium iodide (PI)-mediated DNA staining. This revealed a significant (P = 0.021) reduction in the G_0 fraction ($Ki67^{low}PI^{low}$) in treated cells, and an increase in the $S/G_2/M$ phase (Fig. 3A). Furthermore, MRT403 treatment resulted in reduction in absolute numbers of $CD34^+$ and $CD34^+CD133^+$ CML cells (n=8), suggesting differentiation towards more mature immunophenotype (Fig. 3, B and C).

To further investigate the role of ULK1 in differentiation of CML cells, we cultured primary $CD34^+$ CML cells (n=3) with additional low concentrations (3U/mL) of erythropoietin (EPO), which sensitises primitive blood cells to erythroid lineage commitment. Using expression of surface markers CD45RA and CD123, we next assessed the ratio of common myeloid progenitor (CMP), granulocyte-macrophage progenitor (GMP) and megakaryocyte/erythroid progenitor (MEP) cell populations following treatment with MRT403, using a high concentration of EPO (γEPO; 25U/mL) as a positive control for potent erythroid differentiation. This demonstrated that prolonged treatment with high concentration of EPO resulted in an expansion of the MEP population, measured by gradual loss of CD45RA and CD123 expression. (Fig. 3D). However, using these markers time-dependent differentiation following MRT403 was less apparent.

Therefore, we next asked whether MRT403 treatment increases erythropoiesis. $CD34^+$ CML cells (n=4) were treated with MRT403 and stained for markers of erythroid maturation; GlycophorinA (GlyA), found in the erythrocytes membrane, CD71 (transferrin receptor 1), mediates the uptake of transferrin-iron complexes, CD36, a glycoprotein expressed on the surface of erythrocytes and CD44, which expression is lost on the surface of erythrocytes (*40*). Following continuous MRT403 treatment, erythroid maturation was noticeable with increased expression of GlyA, CD71 and CD36 markers, and loss of CD44 expression (Fig. 3, E to G). This effect was reduced with the addition of NAC, suggesting ROS-dependent erythroid differentiation. Following macroscopic examination, it was evident that a proportion of MRT403 treated cells had turned red, indicating increased haemoglobin production, in keeping with increased erythroid maturation (Fig. 3H). Similar results were obtained following ULK1 deletion in K562 cells (fig. S3, G and H), which are known to persist in culture in an undifferentiated state, but can spontaneously differentiate toward early-stage erythrocytes, granulocytes or monocytes (*41*). Taken together, these data demonstrate that ULK1 inhibition alters the metabolic state and increases oxidative stress in primitive CML cells, driving loss of quiescence and increased myeloid differentiation.

MRT403 Treatment Inhibits TKI-Induced Autophagy and Selectively Targets CML LSCs Ex Vivo

The notion that ULK1 activity was important for maintaining primary CML cells in a quiescent and less differentiated stage prompted us to examine whether MRT403 treatment sensitises persistent CML LSCs to TKI treatment. The TKI nilotinib induced autophagy in primary CML cells, indicated by reduction in p62 amounts and changes in LC3B-II amounts (Fig. 4, A and B). MRT403 treatment blocked nilotinib-induced autophagy, evident by the accumulation of p62. Similar results were obtained when either MRT403 or MRT68921-mediated ULK1 inhibition was

combined with nilotinib treatment in KCL22 cells (fig. S4, A and B). For comparison, similarly to Fig. S2J-K, HCQ partially inhibited autophagy at 3μM, but required 10μM concentration to fully inhibit TKI-induced autophagy, evidenced by accumulation of LC3B-II (fig. S4C). We next observed the fate of primitive CML cells following combined BCR-ABL and ULK1 inhibition. Although MRT403 alone had no effect on CFC numbers, it significantly ($P < 0.001$, n=7*)* enhanced the effect of nilotinib on CML progenitor cells (Fig. 4C). We next performed long-term culture-initiating cell (LTC-IC) assays, using $CD34^+$ cells (n=4). This most stringent ex vivo stem cell assay demonstrated that combined MRT403 and nilotinib treatment significantly ($P = 0.002$) reduced the number of colonies when compared with nilotinib alone (Fig. 4D), indicating that ULK1-mediated autophagy inhibition promoted eradication of primitive CML cells when combined with TKI treatment. Similar results were obtained using MRT68921-mediated ULK1 inhibition in primary CML cells (fig. S4, D and E).

To anticipate possible myelosuppression in humans, we assessed the effect of MRT403 and nilotinib on primitive non-leukaemic haematopoietic human cells. Guided by previous results, normal $CD34^+$ cells were treated with 3μM MRT403, alone or in combination with nilotinib. This revealed no effect of single MRT403 treatment on primary $CD34^+$ cells (n=5) when compared with untreated cells, in contrast to cells treated with omacetaxine mepesuccinate (OMA), an FDA-approved inhibitor of protein biosynthesis, used on occasion for advanced phases of CML (Fig. 4, E and F). In contrast, MRT68921 significantly ($P < 0.001$) reduced CFC and LTC-IC potential of normal cells when used at concentration above 3μM (fig. S4, F and G). Furthermore, whereas increasing the concentration of MRT403 alone did not affect CFC potential of ULK1-competent or ULK1-KO cells, MRT68921 treatment reduced colony formation independently of the presence of ULK1, further highlighting the increased specificity of MRT403 (Fig. 4, G and H).

MRT403 Targets Human CML LSC Xenografts when Combined with TKI Treatment

We next tested the target engagement and anti-leukaemic effect of MRT403 in vivo. A dose finding study demonstrated that a daily dose of ≥10mg/kg (QD, oral gavage) resulted in >1µg/mL concentration (>2µM) of MRT403 in circulating plasma of mice (table S3). A 40mg/kg dose was used in subsequent experiments. To evaluate MRT403 specificity in vivo, control and ULK1 KO cells were transplanted into non-irradiated immunocompromised mice. Mice were then left untreated or treated for 4 weeks with MRT403. MRT403 treatment significantly (P = 0.0029) reduced the number of tumours in mice transplanted with control cells (Fig. 5A). However, MRT403 treatment had no effect on the number of tumours in mice transplanted with ULK1 KO cells, indicating that the anti-tumour effects of MRT403 were mediated through ULK1 inhibition. To assess autophagy inhibition in BM-located human CML cells, we moved to a robust CML xenotransplantation model. Initially, primary $CD34^+$ CML were transplanted into four sub-lethally irradiated mice. 4 weeks following transplantation, mice were treated for 5 days with vehicle or MRT403 (Fig. 5B). p62 and ETC complex IV in isolated human $CD45^+$ leukocytes were used as pharmacodynamic (PD) biomarkers to indicate autophagy/mitophagy inhibition and on-target effect of MRT403 (Fig. 5C and fig. S5A-B). To allow for intra-experimental and intra-patient variability of human xenografts, we next performed two separate PDX studies using two different immunocompromised mouse models and independent primary CML samples. As previously demonstrated, increased human chimerism was achieved by using female $NRGW^{41}$ (NOD.Cg-*Rag1*^{tm1Mom}*Kit*$^{W\text{-}41J}$*Il2rg*^{tm1Wjl}) mice (*42*), when compared with male $NRGW^{41}$ or conventionally used NSG (NOD-Prkdc$^{scid/scid}$-IL2Rγc$^{-/-}$) mice (fig. S5, C and D). After ensuring long-term BM engraftment of human cells, we treated the mice daily starting 9-12 weeks after transplantation for a period of 4 weeks with vehicle only, MRT403 (40mg/kg QD), imatinib (50mg/kg BID) or both

drugs in combination. In all experimental arms, no signs of toxicity were observed during treatment as indicated by mouse weight and BM cellularity, confirming excellent tolerability (Fig. 5, D and E). In line with our previous results using the PDX model (*43*), imatinib had no effect on survival of primitive $hCD45^+CD34^+CD133^+$ cells. Although MRT403 did not have significant effect as a single agent, it significantly ($P = 0.0018$, $P = 0.0043$) reduced the number of CML LSCs when combined with imatinib when compared with untreated or imatinib only arms, respectively (Fig. 5F).

Combination of MRT403 and TKI Treatment Selectively Targets *Bcr-Abl*$^+$ Stem Cells in a Murine CML Model

To complement the PDX work, and to further investigate the effect of MRT403-mediated autophagy inhibition on leukaemogenesis, we turned to an inducible CML mouse model. Using this transplantable model, mice develop leukaemia following *Bcr-Abl* induction in HSCs, indicated by an increase in myeloid cells, splenomegaly and anaemia, resembling human CML (*44*). BM cells were isolated from *Bcr-Abl*$^+$ CD45.2 donor mice and transplanted into sub-lethally irradiated CD45.1 recipient mice (n=27). Following engraftment and irradiation recovery, *Bcr-Abl* was switched on by removing tetracycline from mice drinking water for 10 days and separate mouse cohorts were treated with vehicle control, imatinib, equimolar concentration of MRT403 and HCQ, alone or in combination with imatinib for 4 weeks (Fig. 6A). Splenomegaly was evident in leukaemic mice, which was reverted in mice receiving imatinib alone, and when combined with MRT403 or HCQ (fig. S6A). Whereas a significant ($P = 0.0327$) reduction in the BM-located leukaemic (CD45.2) donor cells was visible in mice receiving a combination of MRT403 and imatinib, the HCQ and imatinib combination was ineffective at reducing BM-located leukaemic donor cells (Fig. 6B). The high percentage of engraftment of *Bcr-Abl*$^+$ cells using this model

(>95% chimerism; fig. S6B) permits measurements of the most primitive leukaemic cell population following single and combination drug treatments. Analysis of CD45.2 $Lin^{-}Sca1^{+}c\text{-}Kit^{+}$ (LSK) cell sub-populations revealed that imatinib treatment enriched for BCR-ABL^{+} long-term (LT)-LSCs, in agreement with previously published work (*31*) (Fig. 6C). The enrichment in LT-LSCs following imatinib therapy was not visible when MRT403 was combined with imatinib treatment, suggesting MRT403 may target BM-located LT-LSCs in vivo. To confirm the detrimental effect on the leukaemia potential of the primitive leukaemia-initiating stem cells, we performed a secondary transplantation experiment where CD45.2 BM cells from primary recipients were harvested and transplanted into sub-lethally irradiated CD45.1 mice (n=26), together with $5x10^5$ CD45.1 carrier cells to avoid BM failure in the secondary recipient mice (Fig. 6A). As expected, limited long-term engraftment of CD45.2 cells was evident in mice receiving BM from vehicle and MTR403 treated donor mice due to reduced number of LT-LSCs in BM of mice with high leukaemia burden (*45*) (Fig 6D). In contrast, leukaemia, defined as >40% long-term CD45.2 engraftment and splenomegaly (>0.005 spleen/body weight ratio), was apparent in 70% of mice receiving BM cells from imatinib treated mice (Fig 6, D to F), in line with the increased number of LT-LSCs in these mice (Fig 6C). Long term engraftment of CD45.2 cells, and leukaemia development, was completely reverted in mice transplanted with BM cells from MRT403+imatinib treated mice, confirming that the combination of ULK1 inhibition and imatinib treatment targets CML LSCs.

To further explore the anti-leukaemic effect of MRT403 and imatinib combination, a separate cohort of mice was transplanted with CD45.2 BM cells and treated for 4 weeks as in the previous set of experiments. The rate of relapse and leukaemia development was then evaluated by measuring survival following drug withdrawal. Imatinib monotherapy had no effect on overall

survival, suggesting rapid relapse following drug withdrawal (Fig 6G). However, the combination of MRT403 and imatinib significantly (P =0.0055) prolonged survival of recipient mice, providing further evidence that this combination approach targets the primitive LSC population that fuels the disease.

No changes were observed in progenitor and HSC populations when recipient mice were treated with MRT403 following transplantation with *Bcr-Abl* negative CD45.2 BM cells, confirming MRT403's limited effect on primitive non-leukaemic cells (fig. S6, C to E). These results suggest a specific role for ULK1 in drug resistance and encouraged us to examine further the consequence of pharmacological or genetic ULK1 inhibition on autophagy and energy homeostasis in CML cells.

Combination of MRT403 and TKI Treatment Restores Erythropoiesis in a Murine CML Model

Next, we wanted to further investigate the role of ULK1 in myeloid skewing in CML cells in vivo using the inducible CML mouse model. We observed an increase in MEPs following combined autophagy and BCR-ABL inhibition (Fig. 7A), with no detectable changes in CMPs or GMPs (fig. S7, A and B). To assess changes in erythroid cells we measured the number of $Ter119^+$ cells in the BM of leukaemic mice. In agreement with figures 3D-3H, this revealed a significant (P = 0.0006) increase in erythroid cells following MRT403 and imatinib combination treatment, reaching a similar amount to that seen in the BM untreated healthy (*Bcr-Abl* OFF) mice (Fig. 7B). This was also demonstrated by an overall increase in the ratio of erythroid cells to more immature $Gr\text{-}1^+/Mac\text{-}1^+$ myeloid cells in leukaemic mice treated with MRT403 and imatinib (Fig. 7C). Haemotoxylin and Eosin (H&E) staining of femur BM sections harvested from mice in each treatment arm revealed dense staining of vascular space or enucleated erythrocytes (cytoplasmic

pink staining) in the BM of mice treated with MRT403 and imatinib combination (Fig. 7D). Gr-1 and Ter119 staining further confirmed that whereas untreated mouse BM contained increased numbers of immature myeloid cells and decreased numbers of erythroid cells, mouse BM treated with MRT403 and imatinib presented with myeloid and erythroid cell ratios similar to non-induced wild type mice (Fig. 7, D to F). To investigate erythroid maturation in more details, we determined distinct stages of in vivo erythropoiesis by using cell surface staining and flow cytometry. This strategy combines expression of Ter119 and CD44 with cell size to quantify terminal erythroid maturation by defining distant erythroid developmental stages: pro-erythroblasts (I), basophilic erythroblasts (II), polychromatic erythroblasts (III), orthochromatic erythroblasts/immature reticulocytes (IV), and mature red blood cells (V) (*40, 46*) (Fig. 7G). We observed an increase in the number of cells in developmental stages II-V in leukaemic mice treated with MRT403 and imatinib, confirming increased overall erythropoiesis in the BM (Fig. 7, H to L). This was also reflected by the proportion of mature red blood cells (region V), which reached 50% in mice treated with MRT403 and imatinib combination (Fig. 7M). Results obtained in MRT403-treated mice transplanted with *Bcr-Abl* negative BM cells indicated no changes in CMP/GMP/MEP populations or in the ratio of erythroid/immature myeloid cells (fig. S7, C to F). However, a reduction was observed in absolute number of $Ter119^{+}$ cells (fig. S7G), reflecting the reduction in pro-erythroblasts, basophilic erythroblasts, polychromatic erythroblasts, and orthochromatic erythroblasts/immature reticulocytes (region I-IV), although this did not significantly change the overall proportion of each developmental stage (fig. S7, H to M). Taken together, this suggests that the effect of pharmacological autophagy inhibition on erythrocyte development is distinct in *Bcr-Abl* expressing cells compared to non-transformed cells.

DISCUSSION

Autophagy has been shown to be required for growth of rat sarcoma virus (RAS) driven cancer cells (*47, 48*), and is also frequently induced as a survival mechanism against anti-cancer treatments, such as chemotherapy, radiotherapy, and targeted therapy, contributing to drug resistance (*2*). For example, cancer cells with activating RAS mutations, such as pancreatic and colorectal cells, exhibit dependence on autophagy as a resistance mechanism following inhibition of the mitogen-activated protein kinase (MAPK) signalling pathway (*49-51*). This provided a rationale for testing the anti-malarial HCQ, a non-specific autophagy inhibitor used in the clinic, in combination with anti-cancer therapy. However, completed clinical trials indicate that treatment with HCQ does not achieve consistent autophagy inhibition in patients when used at maximum tolerated doses (*3-6*). This is increasingly being recognised by academia and industry, driving the pursuit for druggable autophagy targets, and the development of more specific autophagy inhibitors. These efforts have already led to the development of small molecular inhibitors against ULK1 (*10-12*). However, the lack of specificity of these inhibitors is a concern, and compounds suitable for pre-clinical in vivo studies have so far been lacking. Thus, the findings we present here regarding MRT403 report the first pre-clinical ULK1 specific inhibitor that is suitable for animal studies of cancer and other diseases. Moreover, a Phase 1 clinical trial, designed to evaluate the safety, tolerability, and clinical activity of the investigational ULK1 inhibitor CDD-3116, as a single agent and in combination with mitogen-activated protein kinase (MEK) inhibition in patients with RAS driven cancers, has recently been initiated (ClinicalTrials.gov Identifier: NCT04892017). It is hoped that this will further evaluate the concept of ULK1 inhibition as a new treatment option for specific tumour types.

Despite decades of research and increased knowledge about the haematopoietic system, MRD remains a clinical problem in myeloid malignancies. CML is driven by LSCs and represents an ideal tumour type to investigate cancer stem cell biology where findings may be applied to other tumour types. We have recently shown that CML LSCs rely on aberrant oxidative mitochondrial metabolism for survival (*43*). The core function of autophagy is related to metabolism. In this study we show that TKI treatment activates ULK1-dependent autophagy following activation of energy-sensing AMPK, and the increase in autophagy flux supports the survival of therapy resistant CML LSCs when BCR-ABL in inhibited. Furthermore, our study supports the concept that inhibition of ULK1 and autophagy-dependent mitochondrial clearance, also known as mitophagy, in CML models promotes mitochondrial ROS-dependent myeloid differentiation and maturation of erythrocytes.

One limitation in our study is that we did not test the amount of mitochondria clearance during erythropoiesis in CML cells. Studies have indicated that mitophagy plays an important role during erythropoiesis whereby the ablation of ATG7 (*52*), the autophagy receptor NIX (*53*) or ULK1 (*54*) leads to defects in mitochondrial clearance during erythroid maturation. Therefore, it is likely that alternative systems for removing mitochondria are in place when ULK1 is inhibited, supported by the fact that mitochondrial clearance from reticulocytes is diminished, but not completely blocked, in autophagy-deficient erythroid cells (*54, 55*). Since MRT403 inhibits both ULK1 and ULK2, the potential clearance of mitochondria in our system is unlikely to be mediated by residual activity of ULK1-related proteins. This suggests that the way mitochondria are cleared may be context dependent, and potentially regulated by both autophagy-dependent and -independent mechanisms (or non-canonical autophagy pathway), as previously suggested (*55*), or even via mitochondria-derived vesicles, which can be activated following ROS production (*56*). Another limitation in our

study is that the clinical relevance of the increased erythropoiesis following ULK1 inhibition is not clear. Whether combined autophagy inhibition and TKI treatment promotes differentiation of BCR-ABL$^+$ cells or reduces anaemia in individuals with CML, therefore remains to be elucidated.

Resistance of CML LSCs to TKIs has been linked to their undifferentiated and quiescent state. Of clinical relevance, we demonstrated that pharmacological ULK1 inhibition drives differentiation of phenotypically and functionally defined CML stem cells ex vivo and in vivo. This suggests that BCR-ABL expression in LSCs, which is known to drive increased mitochondrial activity (*43*), increased mitochondrial ROS amounts (*57*) and reduced long-term engraftment (*58*) when compared with normal HSCs, makes CML LSCs susceptible to stress-induced differentiation. This exposes a metabolic vulnerability, whereby "exaggeration" of the disease phenotype, in our case through inhibition of mitochondrial clearance, reduces "stemness" and drives CML LSCs out of quiescence. The consequence is sensitisation to TKI treatment, supporting the concept that testing ULK1 inhibitors such as MRT403 or DCC-3116, in combination with TKI treatment is an attractive approach to target LSCs and for CML patients to achieve TFR. Future laboratory and clinical studies should aim to investigate whether pharmacological ULK1 inhibition may also have broader application to related leukaemias, and potentially provide a paradigm for other malignancies with a cancer stem cell hierarchy.

MATERIALS AND METHODS

Study Design

This study was designed to identify and validate effective drug combination to treat CML models that are driven by TKI-resistant CML LSCs. Functional work, including unbiased transcriptional analysis of patient-derived CML cells highlighted ULK1 as a potential target for autophagy inhibition. To this end, we applied CML cell line xenograft model where gene knockout is valuable

for target validation/drug specificity studies (Fig. 1 and 5), CML PDX model, which allows measurements of human CML LSCs following drug treatment (Fig. 5), and transplantable DTG CML model that is suitable for measurements of leukaemia burden and primitive LT-HSCs (Fig. 6). The design of the mouse treatment trials is described below. Mice were transplanted with CML or BM cells by tail vain injection and randomized to the various experimental cohorts at week 1-2 (cell line xenograft), week 9-12 (PDX) or week 4-5 (DTG model). Althougn no statistical methods were used to calculate exact cohort sample size, the number of animals used per arm in each experiment were estimated based on standard deviation measurements in preliminary and previous experiments. To minimize variables for xenograft studies, same sex and similarly aged animals were transplanted with the same number of donor cells. For data analysis, investigators were blinded to the experimental conditions when assessing the outcomes. All mice were cared for equally in an unbiased fashion by animal technicians and investigators and no animal were excluded from the analysis. P values were calculated by method specified in figure legends. In vitro experiments were all performed on at least 3 separate occasions, except where noted.

Primary samples

Primary $CD34^+$ CML samples were obtained from patients with CP-CML (Ph^+) at diagnosis, prior to TKI treatment. $CD34^+$ normal primary samples were surplus cells collected from femoral-head BM, surgically removed from patients undergoing hip replacement. $CD34^+$ cells were isolated using the CD34 MicroBead Kit or CliniMACS (MiltenyiBiotec #130-100-454). Informed consent for all human samples was obtained in accordance with the Declaration of Helsinki and approval of the National Health Service (NHS) Greater Glasgow Institutional Review Board and Clyde Institutional Review Board. Ethical approval for this work has already been granted by the West of Scotland Research Ethics Service (REC reference:15/WS/0077 & 10/S0704/60).

Cell culture

Primary cells were cultured in serum-free medium (SFM) supplemented with SCF (0.2ng/mL; BioLegend #573902), G-CSF (1ng/mL; BioLegend #578602), GM-CSF (0.2ng/mL; BioLegend #572902), IL6 (1ng/mL; BioLegend #570802), MIPα (0.2ng/mL; PeproTech #300-08); LIF (0.05ng/mL; PeproTech #300-05), BIT (20%; STEMCELL Tech. #09500), low-density lipoprotein (40μg/mL; Sigma #L4646), 2-mercaptoethanol (0.1mM; Invitrogen #31350-010), 1% penicillin/streptomycin (LifeTech #15140-122) and resuspended in IMDM (LifeTech #12440-053). The CML cell lines K562 and KCL22 (DSMZ) were cultured in RPMI 1640 medium (LifeTech #11875-093) supplemented with 1% penicillin/streptomycin, 1% L-glutamine and 10% (vol/vol) foetal calf serum. Both primary cells and cell lines were passaged every 2-3 days, maintained at a concentration of $2x10^5$ cells/mL at 37°C with 5% CO_2 and routinely tested for mycoplasma. ULK1 KO single cell cloning was performed with serial dilution in a 96 well plate (100μL/well). Puromycin selection (3μg/mL) was performed following cell expansion and western blotting performed to validate ULK1 KO.

Ex vivo lineage commitment and erythroid maturation

$CD34^+$ CML cells were cultured in SFM media with addition of erythropoietin (EPO; 3U/mL; PeproTech #100-64). Cells were treated for 3, 6 and 9 days with 3μM MRT403 or with DMSO, and media was refreshed every 3 days. 25U/mL of EPO (γEPO) was used as a positive control. Lineage commitment and erythroid maturation was assessed by BD FACSVerse (BD Bioscience) following staining with CD235a (BioLegend #349106), CD71 (BioLegend #334108), CD44 (BioLegend #338804), CD36 (BioLegend #336222), CD123 (BioLegend #306010), CD45RA (BD #347723), CD34 (BD #555824), and CD133 (Miltenyi #130-080-801).

Cell cycle analysis

$CD34^+$ CML were cultured at $2x10^5$ cells/mL and fixed in cold 70% ethanol while vortexed and incubated at -20°C for at least 2h. Cells were then stained with Ki67 (BD #558026) antibody for 20 min. Propidium Iodide was used as a nucleic acid dye.

CFC assay

$3x10^3$ $CD34^+$ cells were seeded in 1.5 mL of Methocult H4034 Optimum (STEMCELL Tech. #04034). For CML cell lines, $1x10^3$ cells were seeded in Methocult 4230 (STEMCELL Tech. #04230). Number of CFCs were counted after 14 days.

LTC-IC assay

Irradiated M2-10B4 and S1/S1 genetically engineered mouse cell lines, expressing human cytokines (feeder cells), were seeded ($7x10^4$ cells each) in Myelocult H5100 (STEMCELL Tech. #05150) supplemented with hydrocortisone in collagen coated plates. The following day, $5x10^4$ primary CML cells (pre-treated for 6 days) were harvested, resuspended in 500µL of Myelocult H5100 and seeded on top of the feeder cells layer and cultured for additional 5 weeks with a weekly refresh of half of the media. Cells were then harvested and transferred to 1.5mL Methocult H4034 Optimum and number of CFC counted after 14 days.

OCR and ECAR measurements

OCR and ECAR were measured using the Seahorse XF96 Flux Analyzer (Seahorse Bioscience). The XF96-well plate was coated with 25µL per well of Cell Tak solution (22.6µg/mL; Corning #354240) and left for at least 30min at room temperature (RT). $CD34^+$ CML cells or KCL22 cells were seeded in each well in 175µL of XF Assay Medium (Seahorse Bioscience #100965–000). For measurements of OCR in KCL22 cells, media was supplemented with 2mM glutamine and 11mM glucose. For $CD34^+$ CML cells, media was supplemented with 2mM glutamine and 25mM

glucose, SCF (0.2ng/mL), G-CSF (1ng/mL), GM-CSF (0.2ng/mL), IL6 (1ng/mL), MIPα (0.2ng/mL); LIF (0.05ng/mL), low-density lipoprotein (40μg/mL), 2-mercaptoethanol (0.1mM), 2mM glutamine. After 30 min in a CO_2-free incubator at 37°C to ensure adherence, the plate was transferred to the Seahorse XF96 analyser. Measurement of OCR was done at baseline and following sequential injections of oligomycin (0.7μM, an ATP synthase inhibitor), FCCP (1.6μM, a mitochondrial uncoupler), antimycin A (1μM, complex III inhibitor) and rotenone (1μM, complex I inhibitor), respectively. Basal respiration relative to untreated was calculated as average of last rate measurements before oligomycin injection minus average of non-mitochondrial respiration rate. For measurements of ECAR, media was prepared as above without glucose. Measurement of ECAR in KCL22 was performed at baseline and following sequential injections of glucose (11mM), oligomycin (0.7μM) and 2-deoxy-glucose (5mM). For $CD34^+$ CML cells, glucose (25mM), oligomycin (0.7μM) and 2-deoxy-glucose (10mM). ECAR relative to untreated calculated as average of maximum measurements before oligomycin injection minus average of last rate measurements before glucose injection.

NADPH measurements

$1x10^6$ cells per condition were harvested and washed in PBS, NADPH was measured and analysed as indicated by the manufacturer (Abcam #ab65349).

ROS measurements

Cells were washed in PBS and stained using 1mL (10μM) of MitoSOX (Thermo Fisher Scientific #M36008) or CellROX (Thermo Fisher Scientific #10422) and incubated for 30min at 37°C. Prior to staining, cells were treated for 1h with 100nM NAC and 1μL 3.7% H_2O_2. Cells were then washed twice in 2mL of PBS and analysed by BD FACSVerse.

Mitochondrial mass measurements

Cells were washed in PBS and stained using 1mL (10μM) of Mitotracker green (MTG, Thermo Fisher Scientific #M7514) and incubated for 30 min at 37°C. Cells were then washed twice in 2mL of PBS and analysed by BD FACSVerse.

DNA damage measurements

$CD34^+$ CML were fixed in cold 70% ethanol while vortexed and incubated at -20°C for at least 2h. Cells were then stained with anti-H2A.X Phospho (Ser139) (BioLegend #613411) antibody for 20 min. DAPI staining was used as a nucleic acid dye.

RT-qPCR

RNA was extracted using PicoPure RNA Isolation Kit (Thermo Fisher Scientific). Reverse transcription was performed with High-Capacity cDNA Reverse Transcription Kit (Thermo Fisher Scientific). TaqMan Array Fast Plates (10μL reaction) were designed to cover a panel of autophagy genes (Thermo Fisher Scientific #4413255-57). Plates containing autophagy primers were used with TaqMan Advanced Fast Master Mix (Thermo Fisher Scientific). The PCR was performed with the following steps: 2min at 50ºC, 10s at 95ºC, followed by 40 cycles at 95ºC for 15s and 60ºC for 30s on C1000 Touch Thermal Cycler (BioRad). The relative mRNA expression was calculated using the ΔΔCT method.

Western blotting

Cells were prepared using lysis buffer containing protease and phosphatase inhibitors. Protein lysates were quantified using BCA protein assay kit (Pierce; Thermo Fisher Scientific #23228) and equilibrated according to standard curve. Lysates were resolved in 8-12% SDS-Page gels. For LC3B analysis, 15% gels were home casted according to BioRad recipe.

Western blotting antibodies

Antibodies from Cell Signaling Technology: AMPKα (1:1,000, #2532), p-AMPK^{Thr172} (1:1,000, #2531), ATG13 (1:1,000, #13468), Crkl (1:500, #3182), p-Crkl^{Tyr207} (1:1,00, #3181), mTOR (1:500, #2983), p-mTOR^{Ser2448} (1:500, #2971), RPS6 (1:1,000, #2317), p-RPS6$^{Ser240/244}$ (1:1,000, #5364), ULK1 (1:1,000, #8054), p-ULK1^{Ser757} (1:500, #6888), p-ULK1^{Ser555} (1:500, #5869), p-ATG13S^{er318}/ATG^{Ser355} (1:1000, #46329), LC3B (1:500, #2775), ATG7 (1:1,000, #8558), GAPDH (1:1,000, #5174), β-tubulin (1:1,000, #2146), Mouse IgG (1:5,000, #7076), Rabbit IgG (1:5,000, #7074). OXPHOS cocktail (1:2,000, Abcam #110413), GFP (1:1,000, Roche #118144600001), MT-CO2 (1:2,000, Thermo #A-6404), p62 (1:1,000, BD #610832), p-ATG13^{Ser318} (1:1,000, Abnova #NBP2-19127).

CRISPR-Cas9 mediated gene editing

To target human ULK1 and ATG7, guides were designed using the optimised tool https://zlab.bio/guide-design-resources. Guides within the first six coding exon and with the highest score and lower probability of off-targets effect were selected. Synthesis of the oligonucleotides was performed by IDT, which were in vitro annealed and cloned in BsmbI digested lentiCRISPRv.2-puro (Addgene #52961). Following stable integration of lentiCRISPRv.2 using lentiviral transfection and 1 week selection using 3μg/mL puromycin, guides were validated by performing western blotting. Oligonucleotides from Addgene:

ATG7 5′-GAAGCTGAACGAGTATCGGC-3′ Addgene

ULK1-15′CGAAGGCGCCGTGGCCGATC3′ Addgene

ULK1-2 5′GCAGCGTCTGAGACTTGGCG3′ Addgene

ULK1-35′AGCAGATCGCGGGCGCCATG3′ Addgene

Lentivirus production

Lentiviruses for pLentiCRISPRv.2 and pLenti CMV V5-LUC blasticidin (Addgene #21474) were produced by calcium phosphate method using pCMV-VSV-G (envelope plasmid) and psPAX2 (packaging constructs) vectors and HEK293FT for transfection. Retroviruses for YFP-Parkin-IRES-zeocin (plasmid donated by Stephen Tait) were produced by transfection of Phoenix-Ampho HEK.

FACS analysis

BM lineage specific markers were assessed using flow cytometry analysis. BM was resuspended in PBS/2%FBS and stained with antibodies for surface specific markers for 20min in the dark. Cells were then washed in PBS and analysed using BD FACSVerse.

Animal studies

Animal work was carried out with ethical approval from the University of Glasgow Animal Welfare and Ethical Review Board (AWERB) under Home Office Licence PPL 60/4492 and personal licence IA68AFD03.

Luciferase bio-imaging

KCL22 control or ULK1 KO cells were transfected with pLenti CMV V5-LUC blasticidin vector using lentiviral transfection and selected based on antibiotic resistance. NSG or NRGW[41] mice transplanted by tail vein injection with control or ULK1 KO cells ($4x10^6$ cells/mouse) were weekly injected sub-cutaneously with 200µL D-luciferin (Perkin-Elmer #122799-2) and analysed by luciferase bioimaging, using an IVIS Spectrum In Vivo Imaging System, to monitor tumour burden. Following engraftment of the cells (10-13 days post-transplant) mice were treated for 4 weeks with either MRT403 (40mg/kg; QD) or imatinib (50mg/kg; BID).

Drug escalation study

Mice were treated daily for 2 weeks with MRT403, with initial dose of 5mg/kg and highest dose of 40mg/kg (dose doubled every 5 days). Blood was harvested performing cardiac puncture following 24h treatment with lowest dose (5mg/kg), after 5 days treatment with 10mg/kg and following 5 days treatment using 40mg/kg, and immediately poured in tubes containing EDTA. Tubes were inverted 3 times to avoid blood clotting. Samples were centrifuged at 2000g/20min at RT to separate plasma from each sample. Plasma was then collected into a fresh tube and stored at -80ºC.

PDX studies

$CD34^+$ CML cells were transplanted by tail vein injection ($1x10^6$ cells/mouse) into 8-12-week-old sub-lethally irradiated (2.25 Gy) female NSG, female/male NRGW41 mice. Following 9-12 weeks post-transplant, mice were treated by oral gavage with vehicle (water+NMP-PEG), MRT403 (40mg/kg; QD), imatinib (50mg/kg; BID) or the combination of MRT403 and imatinib for 4 weeks. Following treatment, BM was extracted from hip, tibia, and femur from each mouse. CD45, CD34 and CD133 expression was measured by FACS analysis.

In vivo autophagy measurements

$CD34^+$ CML cells were transplanted by tail vein injection ($1x10^6$ cells/mouse) into 8 weeks-old sub-lethally irradiated (2.25 Gy) female NRGW41 mice. Following 4 weeks engraftment, mice were treated by oral gavage with either vehicle (water+NMP-PEG), MRT403 (40mg/kg; QD) for 5 days. Mice were then culled, and BM extracted from hip, tibia, and femur from each mouse. Human $CD45^+$ cells were FACS sorted and autophagy/mitophagy markers evaluated by western blotting.

Transgenic mouse model

CD45.2 BM cells harvested from tibia, femurs, and hips of *Scl-tTa–BCR-ABL* mice were transplanted by tail vein injection ($2x10^6$ cells/mouse) into 8 weeks-old sub-lethally irradiated (2x4.25Gy, 3h apart) female and male CD45.1 C57/Bl6 recipient mice. Mice were maintained on tetracycline (0.5g/L) for 3 weeks prior to removal of tetracycline from the drinking water for transgene induction. Following 10-14 days off tetracycline, mice were treated with vehicle (water+NMP-PEG), MRT403 (40mg/kg; QD), HCQ (36mg/kg; QD), imatinib (50mg/kg; BID) or the combinations of MRT403 and imatinib, and HCQ and imatinib, for 4 weeks. Following treatment, BM was extracted from hips, tibias, and femurs from each mouse. For survival study, mice were kept off tetracycline following 4 weeks treatment and culled following 20% loss of total body weight.

Secondary transplant study

CD45.2 BM cells harvested from tibia, femurs, and hips of *Scl-tTa–BCR-ABL* mice following 4 weeks treatment with either vehicle (water+NMP-PEG), MRT403 (40mg/kg; QD), imatinib (50mg/kg; BID) or the combination of MRT403 and imatinib. BM cells ($3x10^6$ CD45.2 cells/mouse, plus $5x10^5$ CD45.1 carrier cells/mouse) were tail vein injected into 8 weeks-old sub-lethally irradiated (2x4.25Gy, 3h apart) female and male CD45.1 C57/Bl6 recipient mice. Mice were maintained off tetracycline (0.5g/L) for 8 weeks. At week 8 mice were culled and BM extracted from hips, tibias and femurs from each mouse and analysed for leukaemia burden.

IHC analysis

Femurs were collected following 4 weeks *in vivo* treatment as indicated above. Four micron– thick sections were prepared and fixed in formalin for 16h, transferred to 70% ethanol and paraffin-

embedded. Bone sections were prepared and stained with H&E, Ter119 (1:400; BD #550565) and Ly6G (1:60000; 2B Scientific #BE0075-1) IHC. Antigen retrieval was performed for 20min using ER2 buffer from Leica and performed on-board the Leica Bond Rx auto-stainer.

Kinase selectivity assay

Compounds were profiled against a panel of 80 kinases at Dundee (Division Signal Transduction Therapy; DSTT) in single point mode at 1μM. ULK1 versus ULK2 kinase activities were compared against selected kinases using a radiometric assay, to measure the incorporation of radiolabelled 33P into kinase substrate using a glass fibre capture filter method. Reaction conditions for ULK1 were 0.2mg/mL MBP, 20μM ATP (0.25μCi/well), 50mM Tris HCl, pH7.5, 10mM MgCl2, 0.1% beta-mercaptoethanol, 0.1mM EGTA, 0.01% BSA. For ULK2 (DSTT, Dundee), 5μM ATP (0.25μci/well) was substituted. AMPK and JAK2 were measured using a mobility shift assay (Caliper EZ Reader II), which measures both substrate peptide and phospho-peptide product. AMPKα2/β1/γ1 (#02-114) and Jak2 (#08-045) were sourced from Carna Biosciences. Reaction conditions were set at 1μM peptide (AMPK peptide – peptide#10 or Jak2 peptide – peptide 22; Caliper Life sciences), Km ATP (50μM and 5μM AMPK and Jak2 respectively), 50mM Tris HCl pH7.5, 0.1mM EGTA, 0.1% beta-mercaptoethanol, 10mM MgCl2. Reactions were incubated at RT and terminated with the addition of 100mM EDTA before more than 10% of the peptide had been phosphorylated. Compounds were tested in duplicate, and values normalised to 3% DMSO only controls. The data were fitted to a four-parameter fit equation and the IC50 values shown are averages of at least two independent experiments.

Statistical Analysis

Raw data obtained from Seahorse XF96 Flux Analyzer, RT-qPCR and FACS analysis assays were copied into Excel (Microsoft) or Prism (GraphPad Software) spreadsheets. Graphs were generated

and statistical analysis performed with Prism. Error bars indicate the S.D. or S.E.M. The number of biological replicates and applied statistical analysis are indicated in the figure legends. All raw numerical data are presented in Data File S1-S14. All mean values, S.D., and S.E.M. values of technical or biological replicates were calculated using the calculator function. Graphical representation was produced in Prism. Statistical significance for data was determined by paired or unpaired Student's T-test. For multiple comparisons, ANOVA and Dunnett's multiple comparisons test was used (logarithmically transformed variables were used in Fig. 1E, 3D-G, 5F, 7M) to meet the assumption of normal distribution). For in vivo work, overall survival was monitored by Kaplan-Meier analysis and *P*-values calculated using Log-rank (Mantel-Cox). For Kaplan-Meier plots, log rank *P*-values are presented.

Supplementary Materials

Fig. S1-S7.

Table S1-S3.

Data File S1-S14

References

1. D. Gatica, V. Lahiri, D. J. Klionsky, Cargo recognition and degradation by selective autophagy. *Nat Cell Biol* **20**, 233-242 (2018); published online EpubMar (10.1038/s41556-018-0037-z).
2. R. K. Amaravadi, A. C. Kimmelman, J. Debnath, Targeting Autophagy in Cancer: Recent Advances and Future Directions. *Cancer discovery* **9**, 1167-1181 (2019); published online EpubSep (10.1158/2159-8290.CD-19-0292).
3. A. Poklepovic, D. A. Gewirtz, Outcome of early clinical trials of the combination of hydroxychloroquine with chemotherapy in cancer. *Autophagy* **10**, 1478-1480 (2014); published online EpubAug (10.4161/auto.29428).
4. N. B. Haas, L. J. Appleman, M. Stein, M. Redlinger, M. Wilks, X. Xu, A. Onorati, A. Kalavacharla, T. Kim, C. J. Zhen, S. Kadri, J. P. Segal, P. A. Gimotty, L. E. Davis, R. K. Amaravadi, Autophagy Inhibition to Augment mTOR Inhibition: a Phase I/II Trial of Everolimus and Hydroxychloroquine in Patients with Previously Treated Renal Cell Carcinoma. *Clin Cancer Res* **25**, 2080-2087 (2019); published online EpubApr 1 (10.1158/1078-0432.CCR-18-2204).
5. T. B. Karasic, M. H. O'Hara, A. Loaiza-Bonilla, K. A. Reiss, U. R. Teitelbaum, E. Borazanci, A. De Jesus-Acosta, C. Redlinger, J. A. Burrell, D. A. Laheru, D. D. Von Hoff, R. K. Amaravadi, J. A. Drebin, P. J. O'Dwyer, Effect of Gemcitabine and nab-Paclitaxel With or Without Hydroxychloroquine on Patients With Advanced Pancreatic Cancer: A Phase 2 Randomized Clinical Trial. *JAMA Oncol* **5**, 993-998 (2019); published online EpubJul 1 (10.1001/jamaoncol.2019.0684).

6. G. A. Horne, J. Stobo, C. Kelly, A. Mukhopadhyay, A. L. Latif, J. Dixon-Hughes, L. McMahon, P. Cony-Makhoul, J. Byrne, G. Smith, S. Koschmieder, T. H. BrUmmendorf, P. Schafhausen, P. Gallipoli, F. Thomson, W. Cong, R. E. Clark, D. Milojkovic, G. V. Helgason, L. Foroni, F. E. Nicolini, T. L. Holyoake, M. Copland, A randomised phase II trial of hydroxychloroquine and imatinib versus imatinib alone for patients with chronic myeloid leukaemia in major cytogenetic response with residual disease. *Leukemia*, (2020); published online EpubJan 10 (10.1038/s41375-019-0700-9).
7. V. W. Rebecca, M. C. Nicastri, C. Fennelly, C. I. Chude, J. S. Barber-Rotenberg, A. Ronghe, Q. McAfee, N. P. McLaughlin, G. Zhang, A. R. Goldman, R. Ojha, S. Piao, E. Noguera-Ortega, A. Martorella, G. M. Alicea, J. J. Lee, L. M. Schuchter, X. Xu, M. Herlyn, R. Marmorstein, P. A. Gimotty, D. W. Speicher, J. D. Winkler, R. K. Amaravadi, PPT1 Promotes Tumor Growth and Is the Molecular Target of Chloroquine Derivatives in Cancer. *Cancer discovery* **9**, 220-229 (2019); published online EpubFeb (10.1158/2159-8290.CD-18-0706).
8. W. E. Dowdle, B. Nyfeler, J. Nagel, R. A. Elling, S. Liu, E. Triantafellow, S. Menon, Z. Wang, A. Honda, G. Pardee, J. Cantwell, C. Luu, I. Cornella-Taracido, E. Harrington, P. Fekkes, H. Lei, Q. Fang, M. E. Digan, D. Burdick, A. F. Powers, S. B. Helliwell, S. D'Aquin, J. Bastien, H. Wang, D. Wiederschain, J. Kuerth, P. Bergman, D. Schwalb, J. Thomas, S. Ugwonali, F. Harbinski, J. Tallarico, C. J. Wilson, V. E. Myer, J. A. Porter, D. E. Bussiere, P. M. Finan, M. A. Labow, X. Mao, L. G. Hamann, B. D. Manning, R. A. Valdez, T. Nicholson, M. Schirle, M. S. Knapp, E. P. Keaney, L. O. Murphy, Selective VPS34 inhibitor blocks autophagy and uncovers a role for NCOA4 in ferritin degradation and iron homeostasis in vivo. *Nat Cell Biol* **16**, 1069-1079 (2014); published online EpubNov (10.1038/ncb3053).
9. B. Ronan, O. Flamand, L. Vescovi, C. Dureuil, L. Durand, F. Fassy, M. F. Bachelot, A. Lamberton, M. Mathieu, T. Bertrand, J. P. Marquette, Y. El-Ahmad, B. Filoche-Romme, L. Schio, C. Garcia-Echeverria, H. Goulaouic, B. Pasquier, A highly potent and selective Vps34 inhibitor alters vesicle trafficking and autophagy. *Nat Chem Biol* **10**, 1013-1019 (2014); published online EpubDec (10.1038/nchembio.1681).
10. K. J. Petherick, O. J. Conway, C. Mpamhanga, S. A. Osborne, A. Kamal, B. Saxty, I. G. Ganley, Pharmacological inhibition of ULK1 kinase blocks mammalian target of rapamycin (mTOR)-dependent autophagy. *J Biol Chem* **290**, 11376-11383 (2015); published online EpubMay 1 (10.1074/jbc.C114.627778).
11. D. F. Egan, M. G. Chun, M. Vamos, H. Zou, J. Rong, C. J. Miller, H. J. Lou, D. Raveendra-Panickar, C. C. Yang, D. J. Sheffler, P. Teriete, J. M. Asara, B. E. Turk, N. D. Cosford, R. J. Shaw, Small Molecule Inhibition of the Autophagy Kinase ULK1 and Identification of ULK1 Substrates. *Mol Cell* **59**, 285-297 (2015); published online EpubJul 16 (10.1016/j.molcel.2015.05.031).
12. K. R. Martin, S. L. Celano, A. R. Solitro, H. Gunaydin, M. Scott, R. C. O'Hagan, S. D. Shumway, P. Fuller, J. P. MacKeigan, A Potent and Selective ULK1 Inhibitor Suppresses Autophagy and Sensitizes Cancer Cells to Nutrient Stress. *iScience* **8**, 74-84 (2018); published online EpubOct 26 (10.1016/j.isci.2018.09.012).
13. C. H. Jung, C. B. Jun, S. H. Ro, Y. M. Kim, N. M. Otto, J. Cao, M. Kundu, D. H. Kim, ULK-Atg13-FIP200 complexes mediate mTOR signaling to the autophagy machinery. *Mol Biol Cell* **20**, 1992-2003 (2009); published online EpubApr (10.1091/mbc.E08-12-1249).
14. N. Hosokawa, T. Hara, T. Kaizuka, C. Kishi, A. Takamura, Y. Miura, S. Iemura, T. Natsume, K. Takehana, N. Yamada, J. L. Guan, N. Oshiro, N. Mizushima, Nutrient-dependent mTORC1 association with the ULK1-Atg13-FIP200 complex required for autophagy. *Mol Biol Cell* **20**, 1981-1991 (2009); published online EpubApr (10.1091/mbc.E08-12-1248).
15. J. Kim, M. Kundu, B. Viollet, K. L. Guan, AMPK and mTOR regulate autophagy through direct phosphorylation of Ulk1. *Nat Cell Biol* **13**, 132-141 (2011); published online EpubFeb (10.1038/ncb2152).
16. D. Egan, J. Kim, R. J. Shaw, K. L. Guan, The autophagy initiating kinase ULK1 is regulated via opposing phosphorylation by AMPK and mTOR. *Autophagy* **7**, 643-644 (2011); published online EpubJun (10.4161/auto.7.6.15123).
17. D. F. Egan, D. B. Shackelford, M. M. Mihaylova, S. Gelino, R. A. Kohnz, W. Mair, D. S. Vasquez, A. Joshi, D. M. Gwinn, R. Taylor, J. M. Asara, J. Fitzpatrick, A. Dillin, B. Viollet, M. Kundu, M. Hansen, R. J. Shaw, Phosphorylation of ULK1 (hATG1) by AMP-activated protein kinase connects energy sensing to mitophagy. *Science* **331**, 456-461 (2011); published online EpubJan 28 (10.1126/science.1196371).
18. J. H. Joo, F. C. Dorsey, A. Joshi, K. M. Hennessy-Walters, K. L. Rose, K. McCastlain, J. Zhang, R. Iyengar, C. H. Jung, D. F. Suen, M. A. Steeves, C. Y. Yang, S. M. Prater, D. H. Kim, C. B. Thompson, R. J. Youle, P. A. Ney, J. L. Cleveland, M. Kundu, Hsp90-Cdc37 chaperone complex regulates Ulk1- and

Atg13-mediated mitophagy. *Mol Cell* **43**, 572-585 (2011); published online EpubAug 19 (10.1016/j.molcel.2011.06.018).
19. I. Dikic, Z. Elazar, Mechanism and medical implications of mammalian autophagy. *Nat Rev Mol Cell Biol* **19**, 349-364 (2018); published online EpubJun (10.1038/s41580-018-0003-4).
20. B. J. Druker, S. Tamura, E. Buchdunger, S. Ohno, G. M. Segal, S. Fanning, J. Zimmermann, N. B. Lydon, Effects of a selective inhibitor of the Abl tyrosine kinase on the growth of Bcr-Abl positive cells. *Nat Med* **2**, 561-566 (1996); published online EpubMay (
21. S. G. O'Brien, F. Guilhot, R. A. Larson, I. Gathmann, M. Baccarani, F. Cervantes, J. J. Cornelissen, T. Fischer, A. Hochhaus, T. Hughes, K. Lechner, J. L. Nielsen, P. Rousselot, J. Reiffers, G. Saglio, J. Shepherd, B. Simonsson, A. Gratwohl, J. M. Goldman, H. Kantarjian, K. Taylor, G. Verhoef, A. E. Bolton, R. Capdeville, B. J. Druker, I. Investigators, Imatinib compared with interferon and low-dose cytarabine for newly diagnosed chronic-phase chronic myeloid leukemia. *N Engl J Med* **348**, 994-1004 (2003); published online EpubMar 13 (10.1056/NEJMoa022457).
22. T. L. Holyoake, G. V. Helgason, Do we need more drugs for chronic myeloid leukemia? *Immunological reviews* **263**, 106-123 (2015); published online EpubJan (10.1111/imr.12234).
23. F. X. Mahon, D. Rea, J. Guilhot, F. Guilhot, F. Huguet, F. Nicolini, L. Legros, A. Charbonnier, A. Guerci, B. Varet, G. Etienne, J. Reiffers, P. Rousselot, C. Intergroupe Francais des Leucemies Myeloides, Discontinuation of imatinib in patients with chronic myeloid leukaemia who have maintained complete molecular remission for at least 2 years: the prospective, multicentre Stop Imatinib (STIM) trial. *Lancet Oncol* **11**, 1029-1035 (2010); published online EpubNov (10.1016/S1470-2045(10)70233-3).
24. T. L. Holyoake, D. Vetrie, The chronic myeloid leukemia stem cell: stemming the tide of persistence. *Blood* **129**, 1595-1606 (2017); published online EpubMar 23 (10.1182/blood-2016-09-696013).
25. R. Latagliata, P. Volpicelli, M. Breccia, F. Vozella, A. Romano, C. Montagna, M. Molica, P. Finsinger, I. Carmosino, A. Serrao, I. Zacheo, M. Santopietro, A. Salaroli, G. Alimena, Incidence of persistent/late chronic anemia in newly diagnosed patients with chronic myeloid leukemia responsive to imatinib. *Am J Hematol* **90**, 105-108 (2015); published online EpubFeb (10.1002/ajh.23879).
26. M. Sakurai, T. Kikuchi, D. Karigane, H. Kasahara, E. Matsuki, R. Hashida, Y. Yamane, R. Abe, Y. Koda, T. Toyama, J. Kato, T. Shimizu, Y. Yokoyama, S. Suzuki, T. Nakamura, S. Okamoto, T. Mori, Renal dysfunction and anemia associated with long-term imatinib treatment in patients with chronic myelogenous leukemia. *Int J Hematol* **109**, 292-298 (2019); published online EpubMar (10.1007/s12185-019-02596-z).
27. A. Hamilton, G. V. Helgason, M. Schemionek, B. Zhang, S. Myssina, E. K. Allan, F. E. Nicolini, C. Muller-Tidow, R. Bhatia, V. G. Brunton, S. Koschmieder, T. L. Holyoake, Chronic myeloid leukemia stem cells are not dependent on Bcr-Abl kinase activity for their survival. *Blood* **119**, 1501-1510 (2012); published online EpubFeb 9 (10.1182/blood-2010-12-326843).
28. A. S. Corbin, A. Agarwal, M. Loriaux, J. Cortes, M. W. Deininger, B. J. Druker, Human chronic myeloid leukemia stem cells are insensitive to imatinib despite inhibition of BCR-ABL activity. *J Clin Invest* **121**, 396-409 (2011); published online EpubJan (10.1172/JCI35721).
29. J. C. Chomel, M. L. Bonnet, N. Sorel, A. Bertrand, M. C. Meunier, S. Fichelson, M. Melkus, A. Bennaceur-Griscelli, F. Guilhot, A. G. Turhan, Leukemic stem cell persistence in chronic myeloid leukemia patients with sustained undetectable molecular residual disease. *Blood* **118**, 3657-3660 (2011); published online EpubSep 29 (10.1182/blood-2011-02-335497).
30. C. Bellodi, M. R. Lidonnici, A. Hamilton, G. V. Helgason, A. R. Soliera, M. Ronchetti, S. Galavotti, K. W. Young, T. Selmi, R. Yacobi, R. A. Van Etten, N. Donato, A. Hunter, D. Dinsdale, E. Tirro, P. Vigneri, P. Nicotera, M. J. Dyer, T. Holyoake, P. Salomoni, B. Calabretta, Targeting autophagy potentiates tyrosine kinase inhibitor-induced cell death in Philadelphia chromosome-positive cells, including primary CML stem cells. *J Clin Invest* **119**, 1109-1123 (2009); published online EpubMay (
31. P. Baquero, A. Dawson, A. Mukhopadhyay, E. M. Kuntz, R. Mitchell, O. Olivares, A. Ianniciello, M. T. Scott, K. Dunn, M. C. Nicastri, J. D. Winkler, A. M. Michie, K. M. Ryan, C. Halsey, E. Gottlieb, E. P. Keaney, L. O. Murphy, R. K. Amaravadi, T. L. Holyoake, G. V. Helgason, Targeting quiescent leukemic stem cells using second generation autophagy inhibitors. *Leukemia* **33**, 981-994 (2019); published online EpubApr (10.1038/s41375-018-0252-4).
32. M. Holtz, S. J. Forman, R. Bhatia, Growth factor stimulation reduces residual quiescent chronic myelogenous leukemia progenitors remaining after imatinib treatment. *Cancer Res* **67**, 1113-1120 (2007); published online EpubFeb 1 (10.1158/0008-5472.CAN-06-2014).
33. S. W. Tait, A. Oberst, G. Quarato, S. Milasta, M. Haller, R. Wang, M. Karvela, G. Ichim, N. Yatim, M. L. Albert, G. Kidd, R. Wakefield, S. Frase, S. Krautwald, A. Linkermann, D. R. Green, Widespread

mitochondrial depletion via mitophagy does not compromise necroptosis. *Cell Rep* **5**, 878-885 (2013); published online EpubNov 27 (10.1016/j.celrep.2013.10.034).
34. A. D. Baudot, M. Haller, M. Mrschtik, S. W. Tait, K. M. Ryan, Using enhanced-mitophagy to measure autophagic flux. *Methods* **75**, 105-111 (2015); published online EpubMar (10.1016/j.ymeth.2014.11.014).
35. I. Tanida, N. Mizushima, M. Kiyooka, M. Ohsumi, T. Ueno, Y. Ohsumi, E. Kominami, Apg7p/Cvt2p: A novel protein-activating enzyme essential for autophagy. *Mol Biol Cell* **10**, 1367-1379 (1999); published online EpubMay (
36. H. Cheong, U. Nair, J. Geng, D. J. Klionsky, The Atg1 kinase complex is involved in the regulation of protein recruitment to initiate sequestering vesicle formation for nonspecific autophagy in Saccharomyces cerevisiae. *Mol Biol Cell* **19**, 668-681 (2008); published online EpubFeb (10.1091/mbc.e07-08-0826).
37. T. Y. Li, Y. Sun, Y. Liang, Q. Liu, Y. Shi, C. S. Zhang, C. Zhang, L. Song, P. Zhang, X. Zhang, X. Li, T. Chen, H. Y. Huang, X. He, Y. Wang, Y. Q. Wu, S. Chen, M. Jiang, C. Chen, C. Xie, J. Y. Yang, Y. Lin, S. Zhao, Z. Ye, S. Y. Lin, D. T. Chiu, S. C. Lin, ULK1/2 Constitute a Bifurcate Node Controlling Glucose Metabolic Fluxes in Addition to Autophagy. *Mol Cell* **62**, 359-370 (2016); published online EpubMay 5 (10.1016/j.molcel.2016.04.009).
38. K. Ito, A. Hirao, F. Arai, K. Takubo, S. Matsuoka, K. Miyamoto, M. Ohmura, K. Naka, K. Hosokawa, Y. Ikeda, T. Suda, Reactive oxygen species act through p38 MAPK to limit the lifespan of hematopoietic stem cells. *Nat Med* **12**, 446-451 (2006); published online EpubApr (10.1038/nm1388).
39. C. Chen, Y. Liu, R. Liu, T. Ikenoue, K. L. Guan, P. Zheng, TSC-mTOR maintains quiescence and function of hematopoietic stem cells by repressing mitochondrial biogenesis and reactive oxygen species. *J Exp Med* **205**, 2397-2408 (2008); published online EpubSep 29 (10.1084/jem.20081297).
40. K. Chen, J. Liu, S. Heck, J. A. Chasis, X. An, N. Mohandas, Resolving the distinct stages in erythroid differentiation based on dynamic changes in membrane protein expression during erythropoiesis. *Proc Natl Acad Sci U S A* **106**, 17413-17418 (2009); published online EpubOct 13 (10.1073/pnas.0909296106).
41. B. B. Lozzio, C. B. Lozzio, E. G. Bamberger, A. S. Feliu, A multipotential leukemia cell line (K-562) of human origin. *Proc Soc Exp Biol Med* **166**, 546-550 (1981); published online EpubApr (10.3181/00379727-166-41106).
42. P. H. Miller, G. Rabu, M. MacAldaz, D. J. Knapp, A. M. Cheung, K. Dhillon, N. Nakamichi, P. A. Beer, L. D. Shultz, R. K. Humphries, C. J. Eaves, Analysis of parameters that affect human hematopoietic cell outputs in mutant c-kit-immunodeficient mice. *Exp Hematol* **48**, 41-49 (2017); published online EpubApr (10.1016/j.exphem.2016.12.012).
43. E. M. Kuntz, P. Baquero, A. M. Michie, K. Dunn, S. Tardito, T. L. Holyoake, G. V. Helgason, E. Gottlieb, Targeting mitochondrial oxidative phosphorylation eradicates therapy-resistant chronic myeloid leukemia stem cells. *Nat Med* **23**, 1234-1240 (2017); published online EpubOct (10.1038/nm.4399).
44. S. Koschmieder, B. Gottgens, P. Zhang, J. Iwasaki-Arai, K. Akashi, J. L. Kutok, T. Dayaram, K. Geary, A. R. Green, D. G. Tenen, C. S. Huettner, Inducible chronic phase of myeloid leukemia with expansion of hematopoietic stem cells in a transgenic model of BCR-ABL leukemogenesis. *Blood* **105**, 324-334 (2005); published online EpubJan 1 (10.1182/blood-2003-12-4369).
45. B. Zhang, Y. W. Ho, Q. Huang, T. Maeda, A. Lin, S. U. Lee, A. Hair, T. L. Holyoake, C. Huettner, R. Bhatia, Altered microenvironmental regulation of leukemic and normal stem cells in chronic myelogenous leukemia. *Cancer Cell* **21**, 577-592 (2012); published online EpubApr 17 (10.1016/j.ccr.2012.02.018).
46. J. Liu, J. Zhang, Y. Ginzburg, H. Li, F. Xue, L. De Franceschi, J. A. Chasis, N. Mohandas, X. An, Quantitative analysis of murine terminal erythroid differentiation in vivo: novel method to study normal and disordered erythropoiesis. *Blood* **121**, e43-49 (2013); published online EpubFeb 21 (10.1182/blood-2012-09-456079).
47. J. Y. Guo, H. Y. Chen, R. Mathew, J. Fan, A. M. Strohecker, G. Karsli-Uzunbas, J. J. Kamphorst, G. Chen, J. M. Lemons, V. Karantza, H. A. Coller, R. S. Dipaola, C. Gelinas, J. D. Rabinowitz, E. White, Activated Ras requires autophagy to maintain oxidative metabolism and tumorigenesis. *Genes Dev* **25**, 460-470 (2011); published online EpubMar 1 (10.1101/gad.2016311).
48. S. Yang, X. Wang, G. Contino, M. Liesa, E. Sahin, H. Ying, A. Bause, Y. Li, J. M. Stommel, G. Dell'antonio, J. Mautner, G. Tonon, M. Haigis, O. S. Shirihai, C. Doglioni, N. Bardeesy, A. C. Kimmelman, Pancreatic cancers require autophagy for tumor growth. *Genes Dev* **25**, 717-729 (2011); published online EpubApr 1 (10.1101/gad.2016111).
49. C. G. Kinsey, S. A. Camolotto, A. M. Boespflug, K. P. Guillen, M. Foth, A. Truong, S. S. Schuman, J. E. Shea, M. T. Seipp, J. T. Yap, L. D. Burrell, D. H. Lum, J. R. Whisenant, G. W. Gilcrease, 3rd, C. C. Cavalieri, K. M. Rehbein, S. L. Cutler, K. E. Affolter, A. L. Welm, B. E. Welm, C. L. Scaife, E. L. Snyder,

M. McMahon, Protective autophagy elicited by RAF-->MEK-->ERK inhibition suggests a treatment strategy for RAS-driven cancers. *Nat Med* **25**, 620-627 (2019); published online EpubApr (10.1038/s41591-019-0367-9).
50. K. L. Bryant, C. A. Stalnecker, D. Zeitouni, J. E. Klomp, S. Peng, A. P. Tikunov, V. Gunda, M. Pierobon, A. M. Waters, S. D. George, G. Tomar, B. Papke, G. A. Hobbs, L. Yan, T. K. Hayes, J. N. Diehl, G. D. Goode, N. V. Chaika, Y. Wang, G. F. Zhang, A. K. Witkiewicz, E. S. Knudsen, E. F. Petricoin, 3rd, P. K. Singh, J. M. Macdonald, N. L. Tran, C. A. Lyssiotis, H. Ying, A. C. Kimmelman, A. D. Cox, C. J. Der, Combination of ERK and autophagy inhibition as a treatment approach for pancreatic cancer. *Nat Med* **25**, 628-640 (2019); published online EpubApr (10.1038/s41591-019-0368-8).
51. C. S. Lee, L. C. Lee, T. L. Yuan, S. Chakka, C. Fellmann, S. W. Lowe, N. J. Caplen, F. McCormick, J. Luo, MAP kinase and autophagy pathways cooperate to maintain RAS mutant cancer cell survival. *Proc Natl Acad Sci U S A* **116**, 4508-4517 (2019); published online EpubMar 5 (10.1073/pnas.1817494116).
52. M. Mortensen, D. J. Ferguson, M. Edelmann, B. Kessler, K. J. Morten, M. Komatsu, A. K. Simon, Loss of autophagy in erythroid cells leads to defective removal of mitochondria and severe anemia in vivo. *Proc Natl Acad Sci U S A* **107**, 832-837 (2010); published online EpubJan 12 (10.1073/pnas.0913170107).
53. I. Novak, V. Kirkin, D. G. McEwan, J. Zhang, P. Wild, A. Rozenknop, V. Rogov, F. Lohr, D. Popovic, A. Occhipinti, A. S. Reichert, J. Terzic, V. Dotsch, P. A. Ney, I. Dikic, Nix is a selective autophagy receptor for mitochondrial clearance. *EMBO Rep* **11**, 45-51 (2010); published online EpubJan (10.1038/embor.2009.256).
54. M. Kundu, T. Lindsten, C. Y. Yang, J. Wu, F. Zhao, J. Zhang, M. A. Selak, P. A. Ney, C. B. Thompson, Ulk1 plays a critical role in the autophagic clearance of mitochondria and ribosomes during reticulocyte maturation. *Blood* **112**, 1493-1502 (2008); published online EpubAug 15 (
55. J. Zhang, M. S. Randall, M. R. Loyd, F. C. Dorsey, M. Kundu, J. L. Cleveland, P. A. Ney, Mitochondrial clearance is regulated by Atg7-dependent and -independent mechanisms during reticulocyte maturation. *Blood* **114**, 157-164 (2009); published online EpubJul 2 (10.1182/blood-2008-04-151639).
56. V. Soubannier, G. L. McLelland, R. Zunino, E. Braschi, P. Rippstein, E. A. Fon, H. M. McBride, A vesicular transport pathway shuttles cargo from mitochondria to lysosomes. *Curr Biol* **22**, 135-141 (2012); published online EpubJan 24 (10.1016/j.cub.2011.11.057).
57. M. Nieborowska-Skorska, P. K. Kopinski, R. Ray, G. Hoser, D. Ngaba, S. Flis, K. Cramer, M. M. Reddy, M. Koptyra, T. Penserga, E. Glodkowska-Mrowka, E. Bolton, T. L. Holyoake, C. J. Eaves, S. Cerny-Reiterer, P. Valent, A. Hochhaus, T. P. Hughes, H. van der Kuip, M. Sattler, W. Wiktor-Jedrzejczak, C. Richardson, A. Dorrance, T. Stoklosa, D. A. Williams, T. Skorski, Rac2-MRC-cIII-generated ROS cause genomic instability in chronic myeloid leukemia stem cells and primitive progenitors. *Blood* **119**, 4253-4263 (2012); published online EpubMay 3 (10.1182/blood-2011-10-385658).
58. B. Zhang, A. C. Strauss, S. Chu, M. Li, Y. Ho, K. D. Shiang, D. S. Snyder, C. S. Huettner, L. Shultz, T. Holyoake, R. Bhatia, Effective targeting of quiescent chronic myelogenous leukemia stem cells by histone deacetylase inhibitors in combination with imatinib mesylate. *Cancer Cell* **17**, 427-442 (2010); published online EpubMay 18 (10.1016/j.ccr.2010.03.011).

Acknowledgments: We would like to thank the Core Services and Advanced Technologies at the Cancer Research UK Beatson Institute (C596/A17196; A31287), with particular thanks to Biological Services Unit and Histology. We thank Valentin Barthet and Joshua Leach for advice with animal and IHC work. We thank all patients and healthy donors who donated samples and National Health Service (NHS) Greater Glasgow and Clyde Biorepository; Alan Hair for sample processing; Tom Gilbey for cell sorting. We thank Connie J Eaves

for providing NRGW41 mice, Stephen Tait for providing YFP-Parkin construct (*33*) and Kevin Ryan for discussion. We would like to dedicate this work in memory of our mentor Tessa L. Holyoake and our colleague Zuzana Brabcova.

Funding: This work was funded by Tenovus Scotland, Leukaemia UK (formerly Leuka), The Kay Kendall Leukemia Fund (KKLF; KKL698 and KKL1069), Blood Cancer UK (formerly Bloodwise; Ref 18006), MRC confidence in Concept 2018 (MC_PC_18048), Cancer Research UK (C57352/A29754), Friends of Paul O'Gorman Leukaemia Research Centre and The Howat Foundation (all to GVH), Stand Up To Cancer campaign for Cancer Research UK (Ref. C55731/A24896) (MC/DV). MMC is supported by Cancer Research UK Glasgow Centre (A25142). A. Ianniciello is a Princess Royal Tenovus Scotland Medical Research Scholar.

Author contributions: Author contributions: A.I., B.S. and G.V.H developed the concept and designed the experiments; A.I. analysed data and performed all experiments except Fig S2A which was performed by M.A.; K.M.R., M.S., M.M.Z., A.D., K.D. and E.R.K. assisted with ex vivo and in vivo studies, including data analysis. Histology was performed by C.N. (Fig. 7D). Z.B. assisted with statistical analysis; A.M.M. and D.V. assisted with in vivo studies; M.C., D.V., and M.A. provided technical or material support; A.I. and G.V.H. wrote the manuscript, and all others reviewed it. D.V., B.S. and G.V.H. supervised the work.

Competing interests: M.C. has received support from Incyte (research funding, speakers bureau, honoraria), Pfizer (speakers bureau, honoraria) and Novartis (advisory board, speakers bureau, honoraria). All other authors declare that they have no conflict of interests.

Data and materials availability: All data associated with this study are present in the paper or Supplementary Materials. Materials in this study will be made available by contacting the corresponding author. MRT403 will be made available to academic researchers by LifeArc upon reasonable request and following completion of material transfer agreement.

Fig. 1. ULK1 is Critical for TKI-Induced Autophagy. (**A**) Western blots showing protein expression and phosphorylation in $CD34^+$ CML cells following 24h 2μM nilotinib treatment (n=4). Mean ± S.D. P-values were calculated using paired Student's T-test. (**B-C**) Western blots showing protein expression and phosphorylation in $CD34^+$ CML cells following 4-24h 2μM nilotinib treatment; representative of n=5 independent patient samples. (**D**) Western blot showing protein expression and phosphorylation in control and ULK1 KO KCL22 cells following 24h 2μM nilotinib or imatinib treatment. (**E**) Fold change in BLI (photon/sec). $NRGW^{41}$ mice were transplanted with $luciferase^+$ KCL22 control and ULK1-KO cells. After 13 days, mice received either vehicle or imatinib (50mg/kg BID) for four weeks via oral gavage. IVIS imaging was performed following 2 weeks treatment. Mean ± S.E.M. P-values were calculated using one-way ANOVA and Dunnett's multiple comparisons test on logarithmically transformed variables. (**F**) Number and representative imagine of extra-medullary tumours harvested from each mouse at experimental end point. Mean ± S.D. P-values were calculated using one-way ANOVA and Dunnett's multiple comparisons test. (**G**) Overall survival was monitored by Kaplan-Meier analysis. P-values were calculated using Log-rank (Mantel-Cox) and refers to control + imatinib versus ULK1 KO + imatinib.

Fig. 2. Inhibition of ULK1 Induces Mitochondrial Respiration and Oxidative Stress. (**A**) Western blots demonstrating mitochondrial protein expression and relative quantification for CV-ATP5A (**B**) in $CD34^+$ CML cells following 24h 3μM MRT403 treatment (n=5). Mean ± S.D. P-values were calculated using paired Student's T-test. (**C**) Representative oxygen consumption rate (OCR) profile and relative basal OCR in $CD34^+$ CML cells following 3 days 3μM MRT403 treatment (n=4). (**D**) Relative basal OCR in untreated KCL22 cells or following 3 days 3μM MRT403 treatment (n=3 independent experiments). (**E**) Representative flow cytometry plots showing measurements of mitochondrial ROS and relative mean fluorescent intensity (MFI) in $CD34^+$ CML cells following 3 days 3μM MRT403 +/- 100nM NAC or 1h H_2O_2 treatment (n=5). (**F**) MFI of mitochondrial ROS in KCL22 cells (n=3 independent experiments). (**G**) Representative extracellular acidification rate (ECAR) profile and relative basal ECAR in $CD34^+$ CML cells following 3 days 3μM MRT403 treatment (n=5). Mean ± S.D. P-values were calculated using paired Student's T-test. (**H**) Relative basal ECAR in KCL22 cells +/- 3 days 3μM MRT403 treatment (n=3 independent experiments). (**I**) Relative NADPH/NADP+ ratio in $CD34^+$ CML cells following 3 days 3μM MRT403 treatment (n=3). For all experiments mean ± S.D. or S.E.M. P-values were calculated using unpaired Student's T-test.

Fig. 3. MRT403-Mediated ULK1 Inhibition Promotes Loss of Quiescence and ROS-Dependent Differentiation. (**A**) Representative flow cytometry plots and G0/G1/S/G2/M cell cycle phase ratio determined using Ki67 and PI staining following 3 days 3µM MRT403 treatment (n=4). Mean ± S.D. P-values were calculated using paired Student's T-test. (**B-C**) Representative flow cytometry plots showing expression of CD34, absolute numbers of $CD34^+$ and $CD34^+CD133^+$ cells relative to untreated following 3 days 3µM MRT403 treatment (n=8). Mean ± S.D. P-values were calculated using paired Student's T-test. (**D**) $CD34^+$ CML samples were exposed to EPO (3U/mL) and expression of surface markers CD45RA and CD123 following 3, 6 and 9 days 3µM MRT403 treatment evaluated; positive control of MEP commitment was performed using γEPO (25U/mL). Representative flow cytometry plots showing expression of CD45RA and CD123 at day 9. CMP/GMP/MEP ratio measured by flow cytometry at 3, 6 and day 9. Mean ± S.E.M on logarithmically transformed variables. (**E-G**) Erythroid maturation was measured monitoring expression of GlyA/CD71/CD36/CD44 following 3-9 days 3µM MRT403 treatment +/- NAC (100mM); positive control of erythroid maturation was performed using γEPO (25U/mL). Representative flow cytometry plots showing expression of GlyA/CD44, CD71/GlyA and CD36/GlyA at day 9. Percentage of $GlyA^+CD44^-$, $CD71^+GlyA^+$ and $CD36^+GlyA^+$ relative to untreated following 3-9 days MRT403 treatment. Mean ± S.E.M. P-values were calculated using paired Student's T-test on logarithmically transformed variables. (**H**) Representative picture of cell pellets following 9 days 3µM MRT403 treatment, or γEPO +/- NAC.

Fig. 4. MRT403 Treatment Inhibits TKI-Induced Autophagy and Targets CML LSCs. (**A**) Western blots showing autophagy protein expression, and quantification (**B**), in $CD34^+$ CML cells exposed to2μM nilotinib, 3μM MRT403 and the combination for 24h (n=4). (**C**) Representative picture of CFC-derived colonies and relative CFC number following exposure of $CD34^+$ CML cells to 2μM nilotinib, 3μM MRT403 and the combination for 3 days (n=7). (**D**) Relative LTC-IC-derived colonies following exposure to 2μM nilotinib, 3μM MRT403 and the combination for 6 days (n=4). (**E**) Representative picture of CFC-derived colonies and relative CFC number following exposure of normal $CD34^+$ cells to 2μM nilotinib, 3μM MRT403, 100nM omacetaxine and the combination of nilotinib and MRT403 for 3 days (n=5). (**F**) Relative LTC-IC-derived colonies following exposure of normal $CD34^+$ cells to 2μM nilotinib, 3μM MRT403 and the combination for 3 days (n=4). (**G-H**) Relative CFC number following 1-5μM MRT403 and MRT68921 treatment in KCL22 cells. For all experiments mean ± S.E.M. or S.D. P-values were calculated using paired Student's T-test.

Fig. 5. MRT403 Targets Human CML LSC Xenografts when Combined with TKI Treatment. (**A**) NRGW41 (Exp#1) or NSG (Exp#2) mice were transplanted with luciferase+ KCL22 control and ULK1-KO cells. After 10-13 days, mice received either vehicle or MRT403 (40mg/kg BID) for four weeks via oral gavage. IVIS imaging was performed following 2 weeks treatment. Number of extra-medullary tumours harvested from each mouse at experimental end point. Mean ± S.D. P-values were calculated using one-way ANOVA and Dunnett's multiple comparisons test. (**B**) Diagram of PDX experimental design: female NRGW^{41} mice were transplanted with human CD34^{+} CML cells and engraftment was allowed to take place for 4 weeks. Mice were then treated in vivo for 5 days with vehicle or MRT403 (40mg/kg) daily. (**C**) Western blot of autophagy and mitochondrial protein expression in purified human CD45^{+} cells following in vivo treatment. (**D**) Change in mice body weights upon drug treatment. (**E**) Absolute number of mouse BM cells engrafted with human CD34^{+} cells 9-12 weeks post-transplant and following 4 weeks in vivo treatment with the indicated drugs. (**F**) CD34^{+} CML cells (CML#5; CML#6) were transplanted into female NSG or female/male NRGW^{41} mice. Following engraftment of LT-LSCs, (9-12 weeks) mice were treated by oral gavage with vehicle, MRT403 (40mg/kg; QD), imatinib (50mg/kg; BID) or the combination for 4 weeks. Absolute number of human CD45^{+}CD34^{+}CD133^{+} following treatment. Mean ± S.D. P-values were calculated using one-way ANOVA and Dunnett's multiple comparisons test on logarithmically transformed variables to meet the assumption of normal distribution. Representative flow cytometry plots showing expression of CD34/CD133 surface markers.

Fig. 6. MRT403 and TKI Combination Selectively Targets LSCs in an Inducible CML Model. (**A**) Diagram of experimental design: C57BL/6 mice were transplanted with $2x10^6$ tetracycline inducible BCR-ABL^+ (double transgenic; DTG) cells following sub-lethal irradiation. Following irradiation recovery (3 weeks) tetracycline was removed from the drinking water to induce BCR-ABL expression for 10 days. Then mice received oral gavage vehicle, MRT403 (40mg/kg; QD), imatinib (50mg/kg; BID) or the combination for 4 weeks. Following 4 weeks in vivo treatment, mice were culled and $3x10^6$ BM was harvested and transplanted into irradiated recipient mice (2˚ recipient). BM of 2nd recipient was analysed following 8 weeks, or survival measured following drug withdrawal. (**B**) Percent of CD45.2 relative to average of vehicle treated mice. Mean ± S.D. P-values were calculated using one-way ANOVA and Dunnett's multiple comparisons test. (**C**) Flow cytometry gating strategy to measure amounts of primitive LSCs. Cells within the CD45.2+ LSK population were further selected based on expression of CD48/CD150 surface markers. Percent of LT-LSC relative to average of vehicle treated mice. Mean ± S.D. P-values were calculated using one-way ANOVA and Dunnett's multiple comparisons test. (**D**) Percent of CD45.2 relative to average of vehicle treated mice. Mean ± S.D. P-values were calculated using one-way ANOVA and Dunnett's multiple comparisons test. (**E**) Spleen weight relative to body weight from each treatment arm. Mean ± S.D. P-values were calculated using one-way ANOVA and Dunnett's multiple comparisons test. (**F**) Ratio of healthy and leukaemic (>40% long-term CD45.2 engraftment; >0.005 spleen/body weight ratio) mice following secondary transplantation. (**G**) Overall survival monitored by Kaplan-Meier analysis. P-values were calculated using Log-rank (Mantel-Cox).

Fig. 7. Combination of MRT403 and TKI Treatment Restores Erythropoiesis. (**A-B**) Absolute number of BM MEPs and Ter119^{+} cells relative to average of vehicle treated mice. Mean ± S.D. P-values were calculated using one-way ANOVA and Dunnett's multiple comparisons test. (**C**) Ratio of BM Gr-1^{+}/Mac-1^{+} and Ter119^{+} cells from each treatment arm. Mean ± S.D. P-values were calculated using one-way ANOVA and Dunnett's multiple comparisons test. (**D**) H&E, Gr-1 and Ter119 stained femurs sections. Scale bars, 50μM. (**E-F**) Quantitation analysis of Gr-1 and Ter119. FoV=Field-of-View. Mean ± S.D. P-values were calculated using one-way ANOVA and Dunnett's multiple comparisons test. (**G**) Flow cytometry plots demonstrating gating strategy to measure erythroid maturation. Cells were first gated on CD45^{-} cells. From GR1 and CD11b excluded cells (Gr-1^{-}CD11b^{-}), lineage^{-}, Ter119^{+} cells were gated and expression of CD44 surface marker used to visualise different stages of erythropoiesis. (**H-L**) Absolute number of BM pro-erythroblasts (region I), basophilic erythroblasts (region II), polychromatic erythroblasts (region III), orthochromatic erythroblasts/immature reticulocytes (region IV) and mature red blood cells (region V). Mean ± S.D. P-values were calculated using one-way ANOVA and Dunnett's multiple comparisons test. (**M**) Ratio of separate erythroid populations (regions I-V) from each treatment arm. Mean ± S.E.M. P-values were calculated using one-way ANOVA and Dunnett's multiple comparisons test on logarithmically transformed variables.

Fig. 1

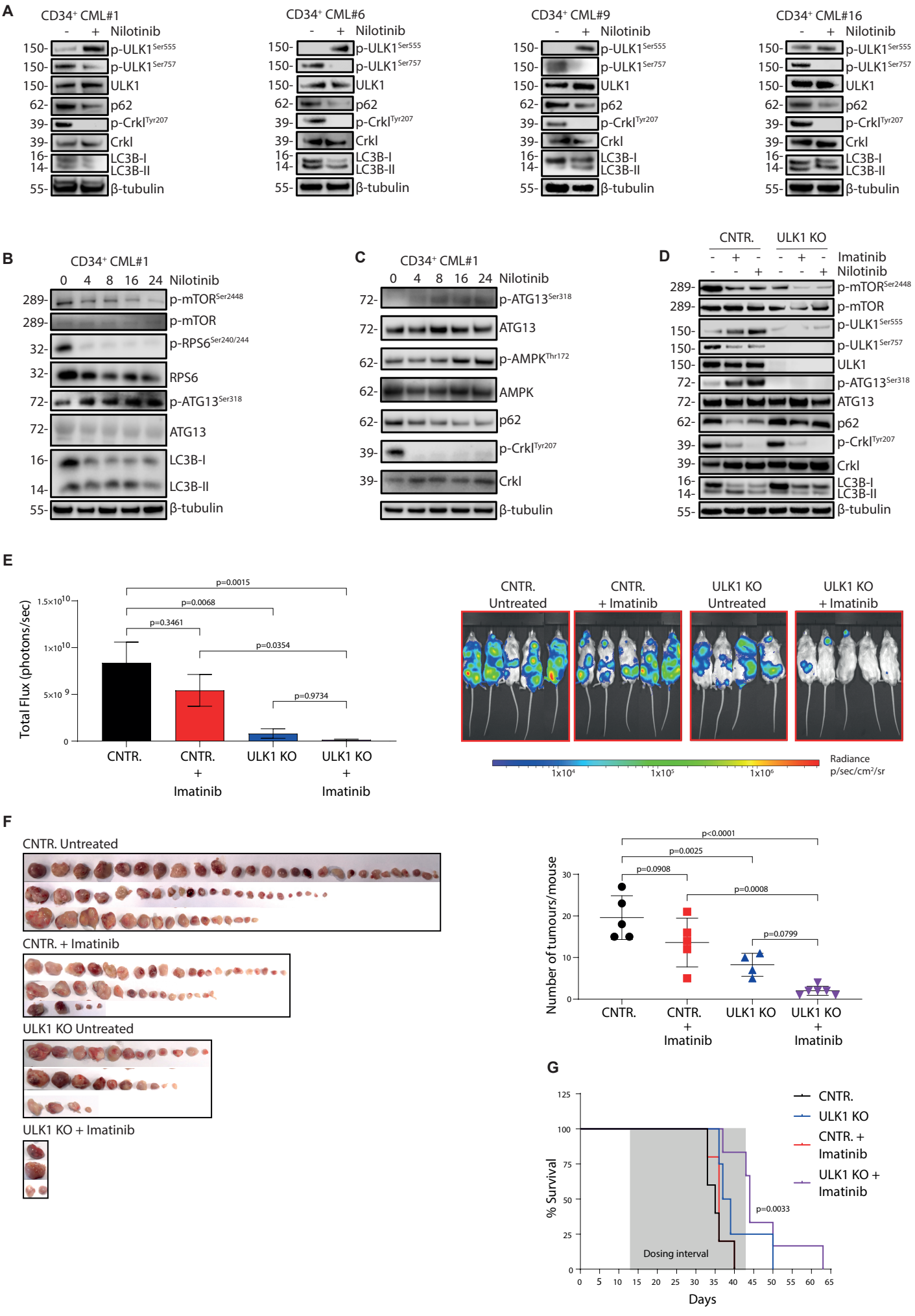
A
CD34+ CML#1
CD34+ CML#6
CD34+ CML#9
CD34+ CML#16
- + Nilotinib
150- p-ULK1Ser555
150- p-ULK1Ser757
150- ULK1
62- p62
39- p-CrkITyr207
39- CrkI
16- LC3B-I
14- LC3B-II
55- β-tubulin
B
CD34+ CML#1
0 4 8 16 24 Nilotinib
289- p-mTORSer2448
289- p-mTOR
32- p-RPS6Ser240/244
32- RPS6
72- p-ATG13Ser318
72- ATG13
16- LC3B-I
14- LC3B-II
55- β-tubulin
C
CD34+ CML#1
0 4 8 16 24 Nilotinib
72- p-ATG13Ser318
72- ATG13
62- p-AMPKThr172
62- AMPK
62- p62
39- p-CrkITyr207
39- CrkI
β-tubulin
D
CNTR.
ULK1 KO
- + - - + - Imatinib
- - + - - + Nilotinib
289- p-mTORSer2448
289- p-mTOR
150- p-ULK1Ser555
150- p-ULK1Ser757
150- ULK1
72- p-ATG13Ser318
72- ATG13
62- p62
39- p-CrkITyr207
39- CrkI
16- LC3B-I
14- LC3B-II
55- β-tubulin
E
Total Flux (photons/sec)
1.5x10^10
1x10^10
5x10^9
0
p=0.0015
p=0.0068
p=0.3461
p=0.0354
p=0.9734
CNTR.
CNTR. + Imatinib
ULK1 KO
ULK1 KO + Imatinib
CNTR. Untreated
CNTR. + Imatinib
ULK1 KO Untreated
ULK1 KO + Imatinib
1x10^4
1x10^5
1x10^6
Radiance p/sec/cm²/sr
F
CNTR. Untreated
CNTR. + Imatinib
ULK1 KO Untreated
ULK1 KO + Imatinib
Number of tumours/mouse
p<0.0001
p=0.0025
p=0.0908
p=0.0008
p=0.0799
G
% Survival
Days
CNTR.
ULK1 KO
CNTR. + Imatinib
ULK1 KO + Imatinib
p=0.0033
Dosing interval

Fig. 2

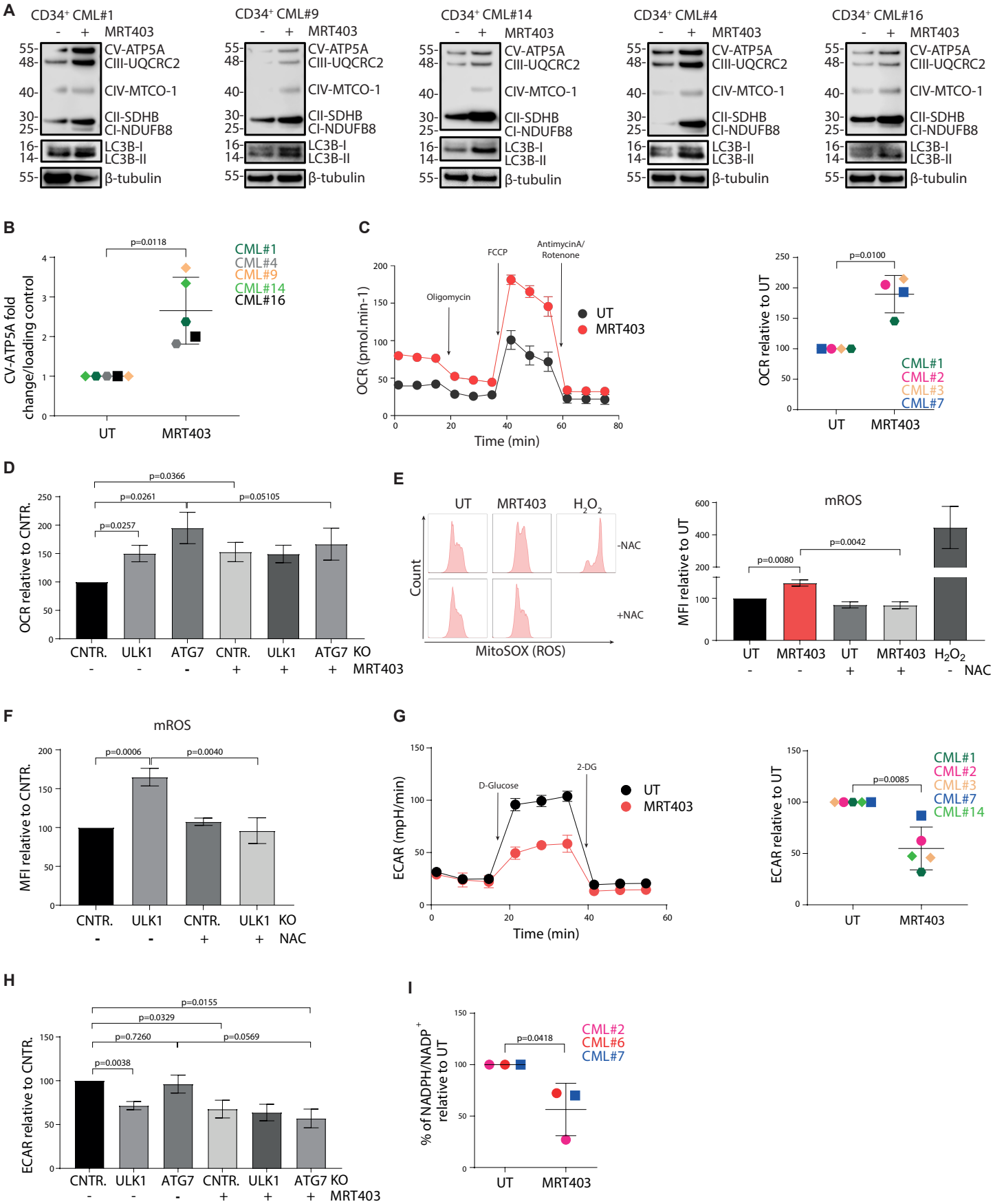
A
CD34+ CML#1
CD34+ CML#9
CD34+ CML#14
CD34+ CML#4
CD34+ CML#16
MRT403
CV-ATP5A
CIII-UQCRC2
CIV-MTCO-1
CII-SDHB
CI-NDUFB8
LC3B-I
LC3B-II
β-tubulin
B
CV-ATP5A fold change/loading control
p=0.0118
CML#1
CML#4
CML#9
CML#14
CML#16
UT
MRT403
C
OCR (pmol.min-1)
Oligomycin
FCCP
AntimycinA/ Rotenone
UT
MRT403
Time (min)
OCR relative to UT
p=0.0100
CML#1
CML#2
CML#3
CML#7
D
OCR relative to CNTR.
p=0.0366
p=0.0261
p=0.05105
p=0.0257
CNTR.
ULK1
ATG7
KO
MRT403
E
UT
MRT403
H2O2
-NAC
+NAC
Count
MitoSOX (ROS)
mROS
MFI relative to UT
p=0.0080
p=0.0042
NAC
F
mROS
MFI relative to CNTR.
p=0.0006
p=0.0040
G
ECAR (mpH/min)
D-Glucose
2-DG
UT
MRT403
Time (min)
ECAR relative to UT
p=0.0085
CML#1
CML#2
CML#3
CML#7
CML#14
H
ECAR relative to CNTR.
p=0.0155
p=0.0329
p=0.7260
p=0.0569
p=0.0038
I
% of NADPH/NADP+ relative to UT
p=0.0418
CML#2
CML#6
CML#7

Fig. 3

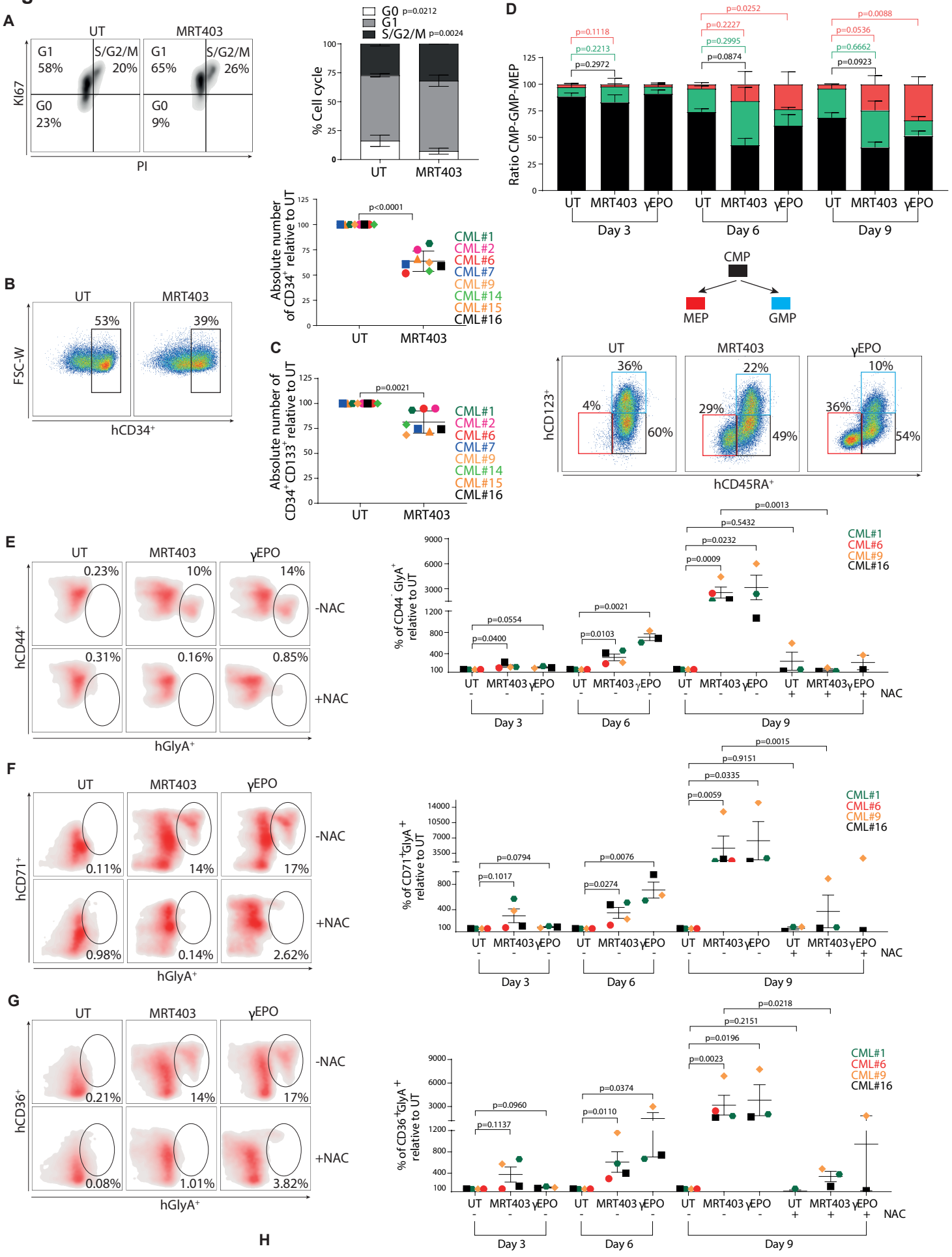
A
UT
MRT403
G1 58%
S/G2/M 20%
G0 23%
G1 65%
S/G2/M 26%
G0 9%
KI67
PI
G0 p=0.0212
G1
S/G2/M p=0.0024
% Cell cycle
UT
MRT403
B
UT
MRT403
53%
39%
FSC-W
hCD34+
Absolute number of CD34+ relative to UT
p<0.0001
CML#1
CML#2
CML#6
CML#7
CML#9
CML#14
CML#15
CML#16
C
Absolute number of CD34+CD133+ relative to UT
p=0.0021
D
Ratio CMP-GMP-MEP
p=0.1118
p=0.2213
p=0.2972
p=0.0252
p=0.2227
p=0.2995
p=0.0874
p=0.0088
p=0.0536
p=0.6662
p=0.0923
UT
MRT403
γEPO
Day 3
Day 6
Day 9
CMP
MEP
GMP
hCD123+
hCD45RA+
36%
4%
60%
22%
29%
49%
10%
36%
54%
E
hCD44+
hGlyA+
0.23%
10%
14%
-NAC
0.31%
0.16%
0.85%
+NAC
% of CD44- GlyA+ relative to UT
p=0.0013
p=0.5432
p=0.0232
p=0.0009
p=0.0554
p=0.0400
p=0.0021
p=0.0103
NAC
F
hCD71+
0.11%
14%
17%
0.98%
0.14%
2.62%
% of CD71+GlyA+ relative to UT
p=0.0015
p=0.9151
p=0.0335
p=0.0059
p=0.0794
p=0.1017
p=0.0076
p=0.0274
G
hCD36+
0.21%
14%
17%
0.08%
1.01%
3.82%
% of CD36+GlyA+ relative to UT
p=0.0218
p=0.2151
p=0.0196
p=0.0023
p=0.0960
p=0.1137
p=0.0374
p=0.0110
H
UT
MRT403
γEPO
UT
MRT403
γEPO
- - - + + + NAC

Fig. 4

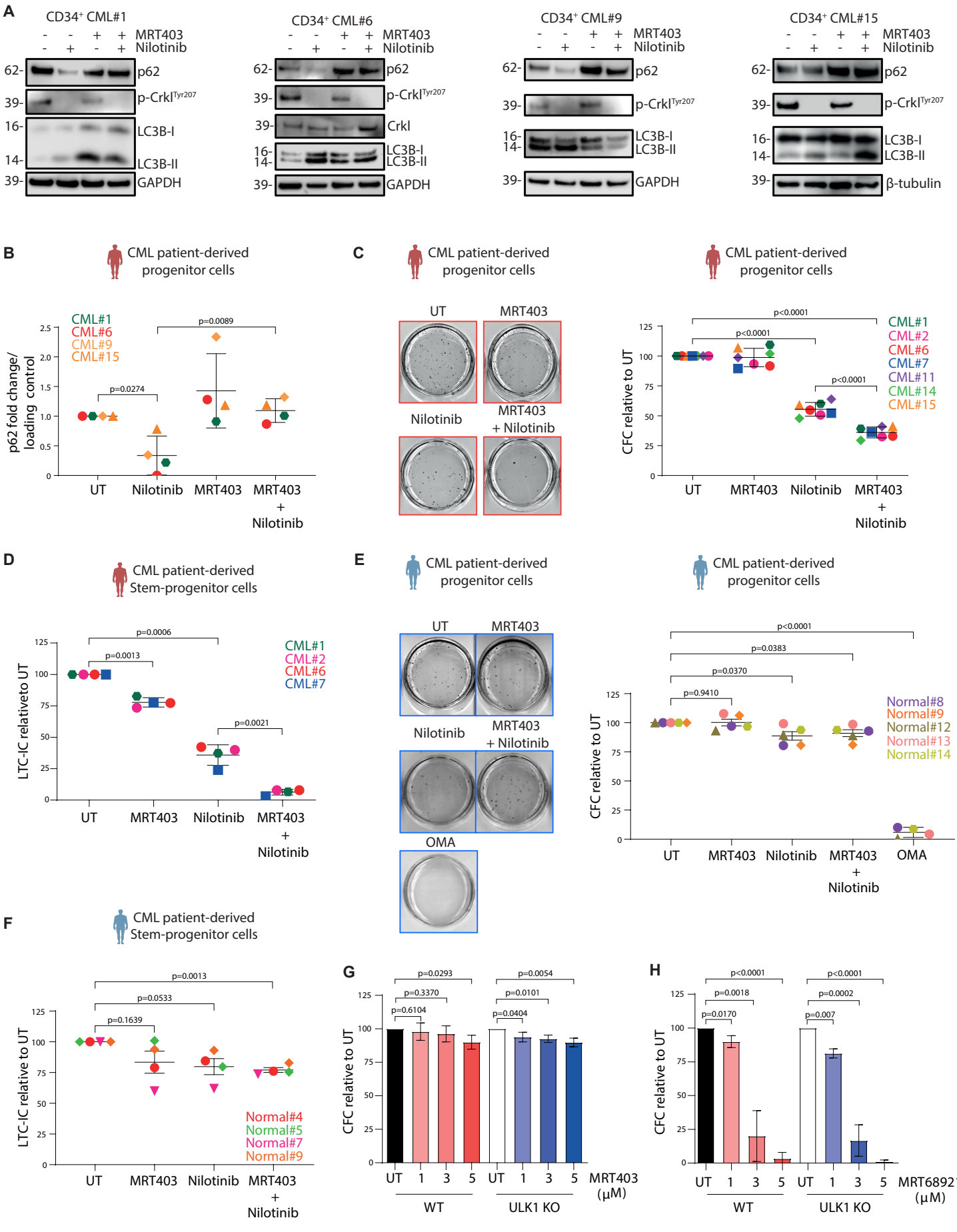
A
CD34+ CML#1
CD34+ CML#6
CD34+ CML#9
CD34+ CML#15
MRT403
Nilotinib
p62
p-CrkI Tyr207
CrkI
LC3B-I
LC3B-II
GAPDH
β-tubulin
B
CML patient-derived progenitor cells
p62 fold change/ loading control
CML#1
CML#6
CML#9
CML#15
p=0.0089
p=0.0274
UT
Nilotinib
MRT403
MRT403 + Nilotinib
C
CML patient-derived progenitor cells
UT
MRT403
Nilotinib
MRT403 + Nilotinib
CFC relative to UT
p<0.0001
CML#1
CML#2
CML#6
CML#7
CML#11
CML#14
CML#15
D
CML patient-derived Stem-progenitor cells
LTC-IC relativeto UT
p=0.0006
p=0.0013
p=0.0021
E
CML patient-derived progenitor cells
OMA
p=0.0383
p=0.0370
p=0.9410
Normal#8
Normal#9
Normal#12
Normal#13
Normal#14
F
CML patient-derived Stem-progenitor cells
LTC-IC relative to UT
p=0.0013
p=0.0533
p=0.1639
Normal#4
Normal#5
Normal#7
Normal#9
G
CFC relative to UT
p=0.0293
p=0.3370
p=0.6104
p=0.0054
p=0.0101
p=0.0404
WT
ULK1 KO
MRT403 (μM)
H
CFC relative to UT
p<0.0001
p=0.0018
p=0.0170
p=0.0002
p=0.007
MRT68921 (μM)

Fig. 5

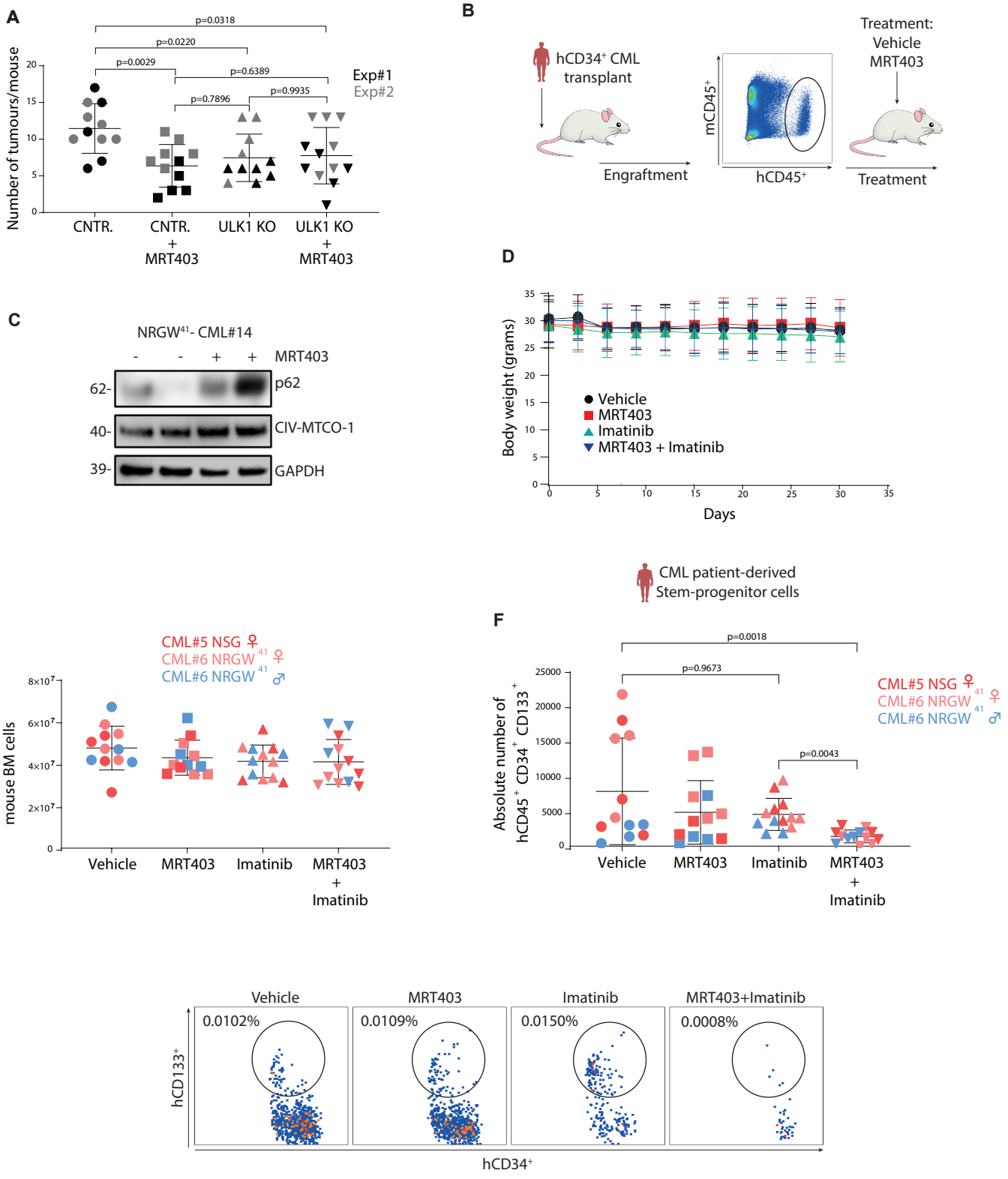
A
p=0.0318
p=0.0220
p=0.0029
p=0.6389
p=0.7896
p=0.9935
Exp#1
Exp#2
Number of tumours/mouse
CNTR.
CNTR. + MRT403
ULK1 KO
ULK1 KO + MRT403
B
hCD34+ CML transplant
Engraftment
mCD45+
hCD45+
Treatment: Vehicle MRT403
Treatment
C
NRGW41- CML#14
- - + + MRT403
62-
p62
40-
CIV-MTCO-1
39-
GAPDH
D
Body weight (grams)
Vehicle
MRT403
Imatinib
MRT403 + Imatinib
Days
CML patient-derived Stem-progenitor cells
E
CML#5 NSG ♀
CML#6 NRGW41 ♀
CML#6 NRGW41 ♂
Absolute number of mouse BM cells
Vehicle
MRT403
Imatinib
MRT403 + Imatinib
F
p=0.0018
p=0.9673
p=0.0043
Absolute number of hCD45+ CD34+ CD133+
CML#5 NSG ♀
CML#6 NRGW41 ♀
CML#6 NRGW41 ♂
Vehicle
MRT403
Imatinib
MRT403 + Imatinib
Vehicle
MRT403
Imatinib
MRT403+Imatinib
0.0102%
0.0109%
0.0150%
0.0008%
hCD133+
hCD34+

Fig. 6

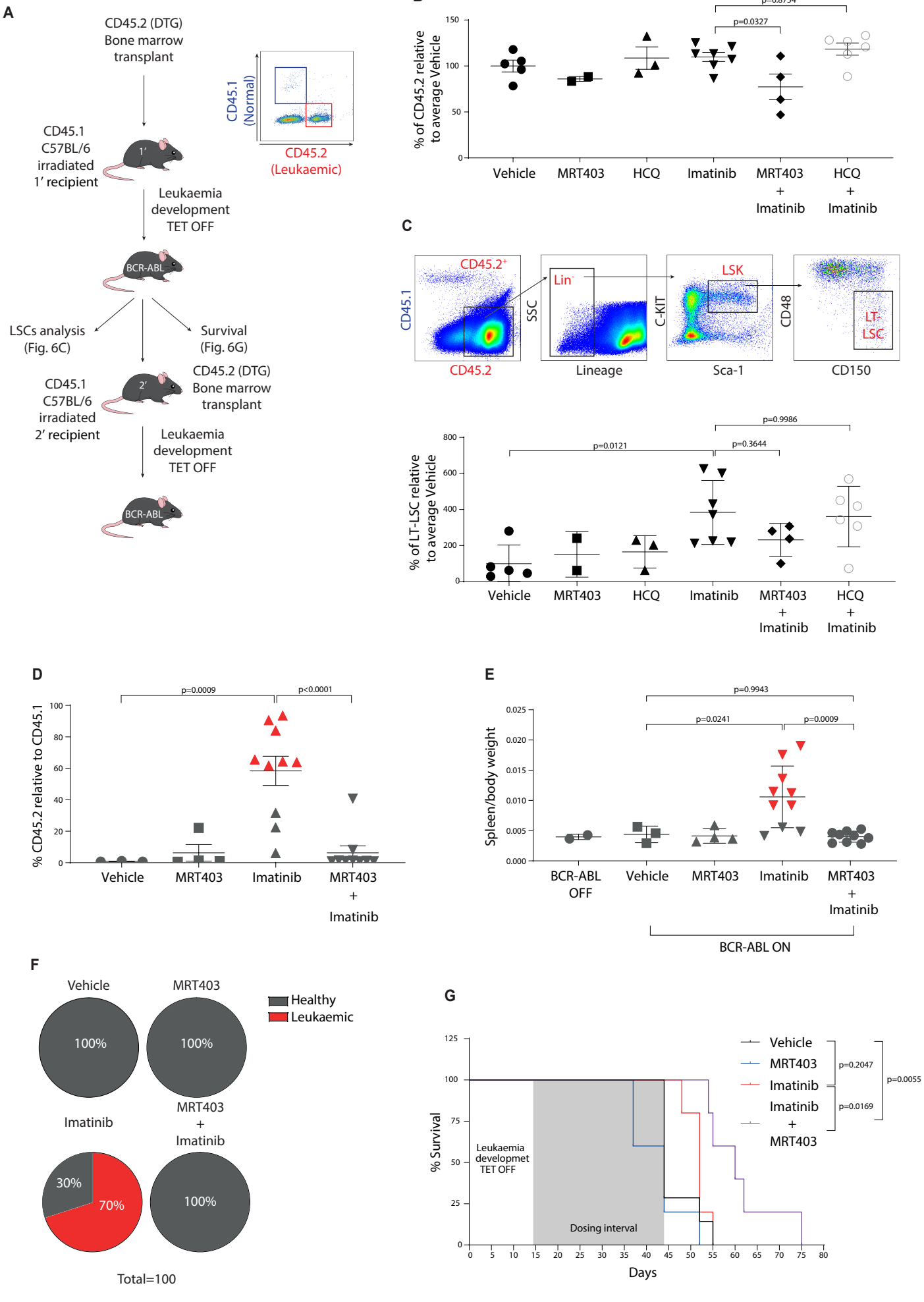
A
CD45.2 (DTG)
Bone marrow
transplant
CD45.1
C57BL/6
irradiated
1′ recipient
1′
CD45.1
(Normal)
CD45.2
(Leukaemic)
Leukaemia
development
TET OFF
BCR-ABL
LSCs analysis
(Fig. 6C)
Survival
(Fig. 6G)
CD45.1
C57BL/6
irradiated
2′ recipient
2′
CD45.2 (DTG)
Bone marrow
transplant
Leukaemia
development
TET OFF
BCR-ABL
B
% of CD45.2 relative
to average Vehicle
p=0.8754
p=0.0327
Vehicle
MRT403
HCQ
Imatinib
MRT403
+
Imatinib
HCQ
+
Imatinib
C
CD45.2+
CD45.1
CD45.2
SSC
Lin-
Lineage
C-KIT
LSK
Sca-1
CD48
LT-
LSC
CD150
% of LT-LSC relative
to average Vehicle
p=0.9986
p=0.0121
p=0.3644
D
% CD45.2 relative to CD45.1
p=0.0009
p<0.0001
E
Spleen/body weight
p=0.9943
p=0.0241
p=0.0009
BCR-ABL
OFF
BCR-ABL ON
F
Vehicle
MRT403
Healthy
Leukaemic
100%
100%
Imatinib
MRT403
+
Imatinib
30%
70%
100%
Total=100
G
% Survival
Leukaemia
developmet
TET OFF
Dosing interval
Days
Vehicle
MRT403
Imatinib
Imatinib
+
MRT403
p=0.2047
p=0.0169
p=0.0055

Fig. 7

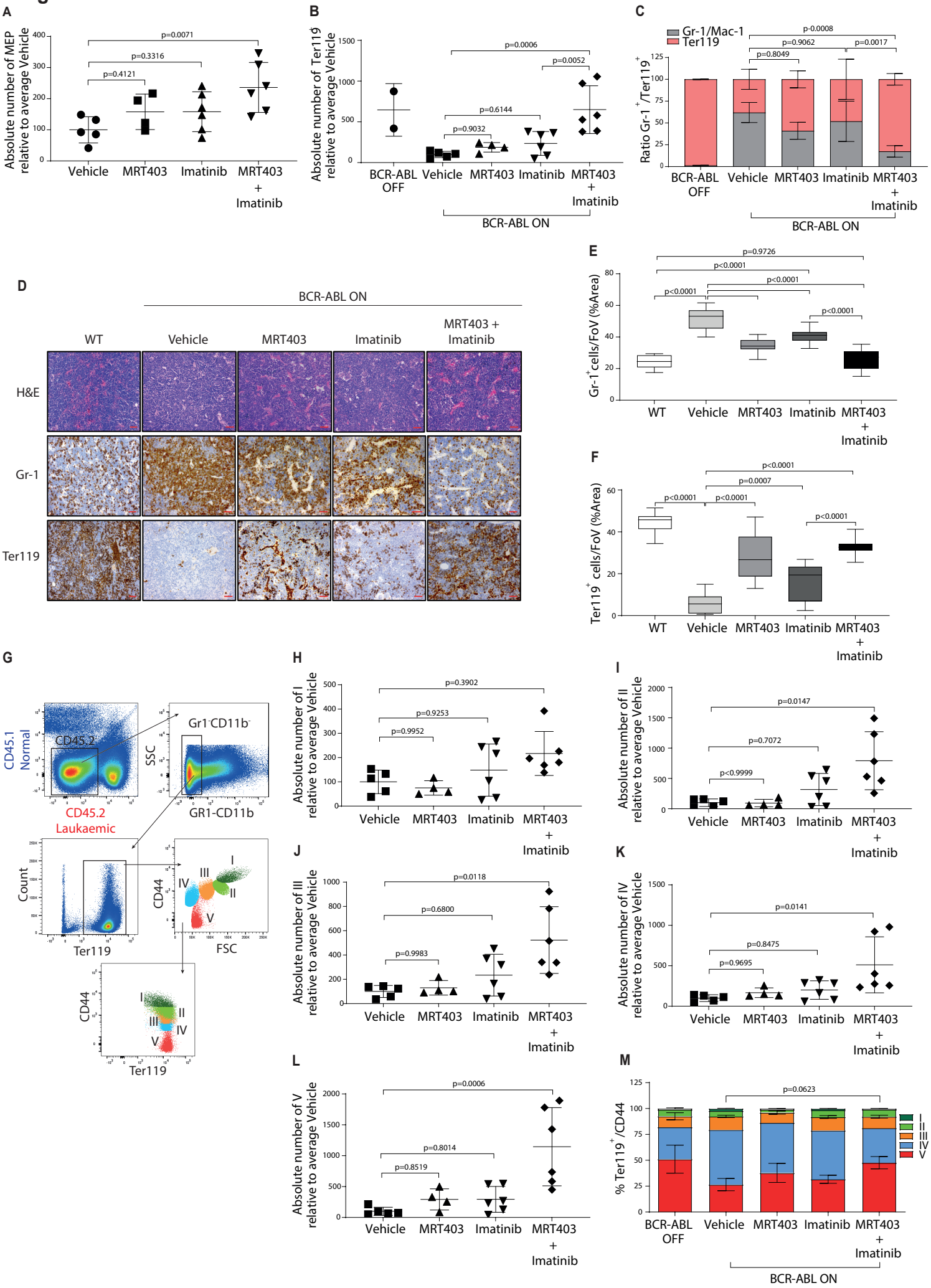
A
Absolute number of MEP relative to average Vehicle
p=0.0071
p=0.3316
p=0.4121
Vehicle
MRT403
Imatinib
MRT403 + Imatinib
B
Absolute number of Ter119+ relative to average Vehicle
p=0.0006
p=0.0052
p=0.6144
p=0.9032
BCR-ABL OFF
Vehicle
MRT403
Imatinib
MRT403 + Imatinib
BCR-ABL ON
C
Gr-1/Mac-1
Ter119
p-0.0008
p=0.9062
p=0.0017
p=0.8049
Ratio Gr-1+/Ter119+
BCR-ABL OFF
Vehicle
MRT403
Imatinib
MRT403 + Imatinib
BCR-ABL ON
D
BCR-ABL ON
WT
Vehicle
MRT403
Imatinib
MRT403 + Imatinib
H&E
Gr-1
Ter119
E
p=0.9726
p<0.0001
p<0.0001
p<0.0001
p<0.0001
Gr-1+cells/FoV (%Area)
WT
Vehicle
MRT403
Imatinib
MRT403 + Imatinib
F
p<0.0001
p=0.0007
p<0.0001
p<0.0001
p<0.0001
Ter119+ cells/FoV (%Area)
WT
Vehicle
MRT403
Imatinib
MRT403 + Imatinib
G
CD45.1 Normal
CD45.2
CD45.2 Laukaemic
Gr1-CD11b-
SSC
GR1-CD11b
Count
Ter119
CD44
FSC
I
II
III
IV
V
H
Absolute number of I relative to average Vehicle
p=0.3902
p=0.9253
p=0.9952
Vehicle
MRT403
Imatinib
MRT403 + Imatinib
I
Absolute number of II relative to average Vehicle
p=0.0147
p=0.7072
p<0.9999
Vehicle
MRT403
Imatinib
MRT403 + Imatinib
J
Absolute number of III relative to average Vehicle
p=0.0118
p=0.6800
p=0.9983
Vehicle
MRT403
Imatinib
MRT403 + Imatinib
K
Absolute number of IV relative to average Vehicle
p=0.0141
p=0.8475
p=0.9695
Vehicle
MRT403
Imatinib
MRT403 + Imatinib
L
Absolute number of V relative to average Vehicle
p=0.0006
p=0.8014
p=0.8519
Vehicle
MRT403
Imatinib
MRT403 + Imatinib
M
% Ter119+/CD44
p=0.0623
I
II
III
IV
V
BCR-ABL OFF
Vehicle
MRT403
Imatinib
MRT403 + Imatinib
BCR-ABL ON

Fig. S1

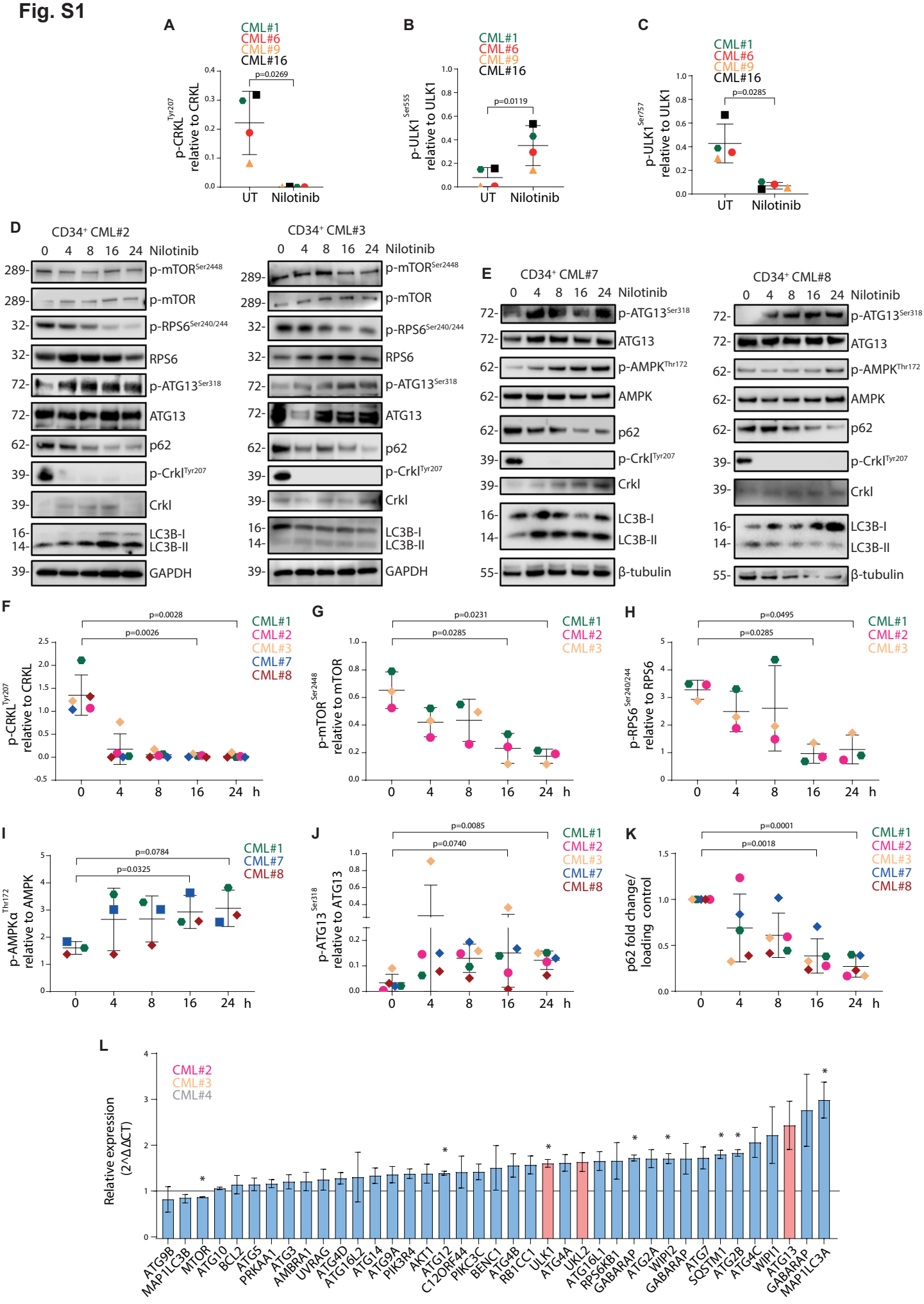
A
CML#1
CML#6
CML#9
CML#16
p=0.0269
p-CRKL Tyr207 relative to CRKL
UT
Nilotinib
B
CML#1
CML#6
CML#9
CML#16
p=0.0119
p-ULK1 Ser555 relative to ULK1
UT
Nilotinib
C
CML#1
CML#6
CML#9
CML#16
p=0.0285
p-ULK1 Ser757 relative to ULK1
UT
Nilotinib
D
CD34+ CML#2
0 4 8 16 24 Nilotinib
p-mTOR Ser2448
p-mTOR
p-RPS6 Ser240/244
RPS6
p-ATG13 Ser318
ATG13
p62
p-CrkI Tyr207
CrkI
LC3B-I
LC3B-II
GAPDH
CD34+ CML#3
0 4 8 16 24 Nilotinib
p-mTOR Ser2448
p-mTOR
p-RPS6 Ser240/244
RPS6
p-ATG13 Ser318
ATG13
p62
p-CrkI Tyr207
CrkI
LC3B-I
LC3B-II
GAPDH
E
CD34+ CML#7
0 4 8 16 24 Nilotinib
p-ATG13 Ser318
ATG13
p-AMPK Thr172
AMPK
p62
p-CrkI Tyr207
CrkI
LC3B-I
LC3B-II
β-tubulin
CD34+ CML#8
0 4 8 16 24 Nilotinib
p-ATG13 Ser318
ATG13
p-AMPK Thr172
AMPK
p62
p-CrkI Tyr207
CrkI
LC3B-I
LC3B-II
β-tubulin
F
p=0.0028
p=0.0026
CML#1
CML#2
CML#3
CML#7
CML#8
p-CRKL Tyr207 relative to CRKL
0 4 8 16 24 h
G
p=0.0231
p=0.0285
CML#1
CML#2
CML#3
p-mTOR Ser2448 relative to mTOR
0 4 8 16 24 h
H
p=0.0495
p=0.0285
CML#1
CML#2
CML#3
p-RPS6 Ser240/244 relative to RPS6
0 4 8 16 24 h
I
p=0.0784
p=0.0325
CML#1
CML#7
CML#8
p-AMPKα Thr172 relative to AMPK
0 4 8 16 24 h
J
p=0.0085
p=0.0740
CML#1
CML#2
CML#3
CML#7
CML#8
p-ATG13 Ser318 relative to ATG13
0 4 8 16 24 h
K
p=0.0001
p=0.0018
CML#1
CML#2
CML#3
CML#7
CML#8
p62 fold change/ loading control
0 4 8 16 24 h
L
CML#2
CML#3
CML#4
Relative expression (2^ΔΔCT)
ATG9B
MAP1LC3B
MTOR
ATG10
BCL2
ATG5
PRKAA1
ATG3
AMBRA1
UVRAG
ATG4D
ATG16L2
ATG14
ATG9A
PIK3R4
AKT1
ATG12
C12ORF44
PIK3C3
BENC1
ATG4B
RB1CC1
ULK1
ATG4A
UKL2
ATG16L1
RPS6KB1
GABARAP
ATG2A
WIPI2
GABARAPL1
ATG7
SQSTM1
ATG2B
ATG4C
WIPI1
ATG13
GABARAPL2
MAP1LC3A

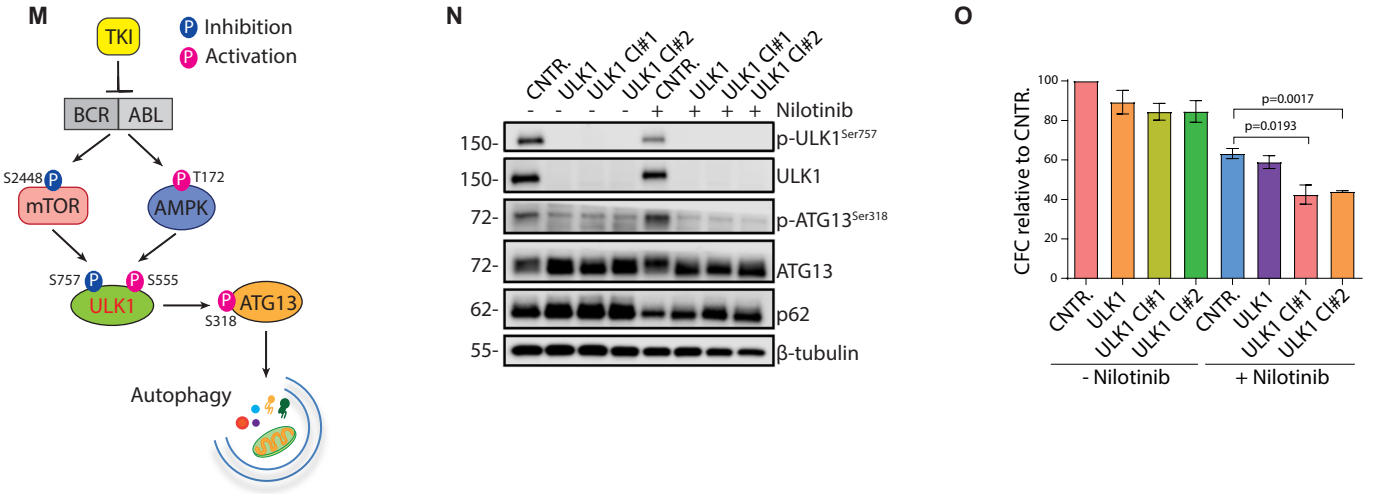
M
TKI
Inhibition
Activation
BCR
ABL
S2448
mTOR
T172
AMPK
S757
S555
ULK1
ATG13
S318
Autophagy
N
CNTR.
ULK1
ULK1 Cl#1
ULK1 Cl#2
CNTR.
ULK1
ULK1 Cl#1
ULK1 Cl#2
- - - - + + + + Nilotinib
150-
p-ULK1Ser757
150-
ULK1
72-
p-ATG13Ser318
72-
ATG13
62-
p62
55-
β-tubulin
O
CFC relative to CNTR.
100
80
60
40
20
0
p=0.0017
p=0.0193
CNTR.
ULK1
ULK1 Cl#1
ULK1 Cl#2
CNTR.
ULK1
ULK1 Cl#1
ULK1 Cl#2
- Nilotinib
+ Nilotinib

Figure S1. ULK1 is Critical for TKI-Induced Autophagy

(**A-C**) Protein phosphorylation quantification in CD34+ CML cells following 24h 2μM nilotinib treatment (n=4). Mean ± S.D. P-values were calculated using paired Student's T-test. (**D-E**) Western blot showing protein expression and phosphorylation, and quantification (**F-K**) in $CD34^+$ CML cells exposed to 2μM nilotinib from 4 to 24h. Mean ± S.E.M. P-values were evaluated using paired Student's T-test. (**L**) . Comparative gene-expression analysis of $CD34^+$ CML cells treated and untreated with nilotinib for 24h. Mean n=3 CML patient samples. Mean ± S.E.M. P-values were evaluated using paired Student's T-test. (**M**) Schematic diagram demonstrating BCR-ABL downstream signalling pathway. (**N**) Western blot showing protein expression and phosphorylation in control and ULK1 KO KCL22 cells following 24h 2μM nilotinib treatment. (**O**) Number of KCL22-derived colonies following ULK KO +/- 72h exposure to 30nM nilotinib. Mean ± S.E.M. P-values were evaluated using unpaired Student's T-test.

Fig. S2

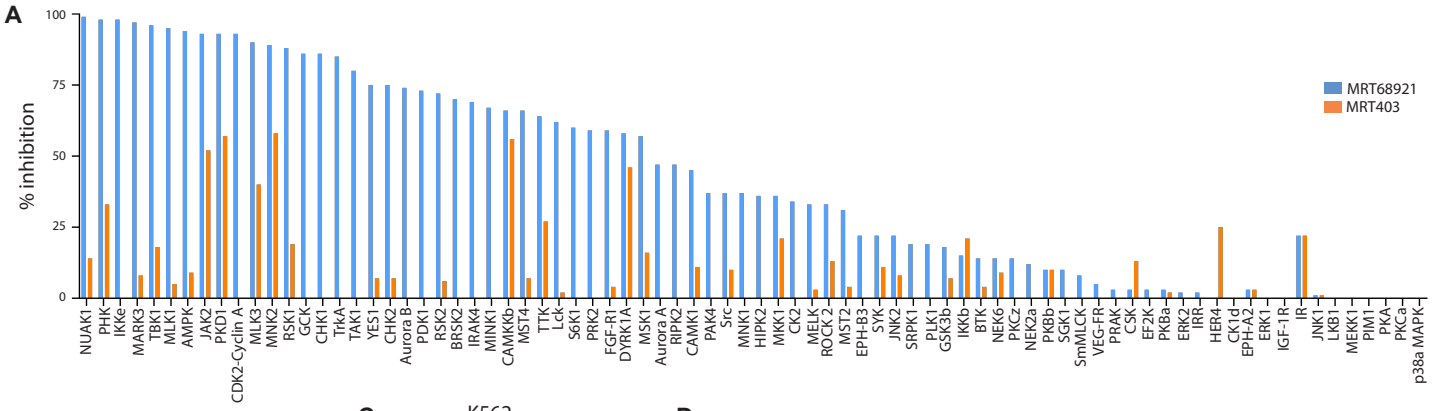
A
% inhibition
MRT68921
MRT403
NUAK1 PHK IKKe MARK3 TBK1 MLK1 AMPK JAK2 PKD1 CDK2-Cyclin A MLK3 MINK2 RSK1 GCK CHK1 TrkA TAK1 YES1 CHK2 Aurora B PDK1 RSK2 BRSK2 IRAK4 MINK1 CAMKKb MST4 TTK Lck S6K1 PRK2 FGF-R1 DYRK1A MSK1 Aurora A RIPK2 CAMK1 PAK4 Src MNK1 HIPK2 MKK1 CK2 MELK ROCK 2 MST2 EPH-B3 SYK JNK2 SRPK1 PLK1 GSK3b IKKb BTK NEK6 PKCz NEK2a PKBb SGK1 SmMLCK VEG-FR PRAK CSK EF2K PKBa ERK2 IRR HER4 CK1d EPH-A2 ERK1 IGF-1R IR JNK1 LKB1 MEKK1 PIM1 PKA PKCa p38a MAPK

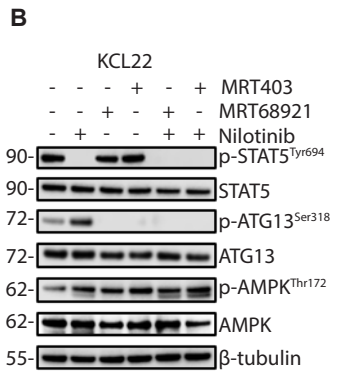
B
KCL22
MRT403
MRT68921
Nilotinib
p-STAT5Tyr694
STAT5
p-ATG13Ser318
ATG13
p-AMPKThr172
AMPK
β-tubulin

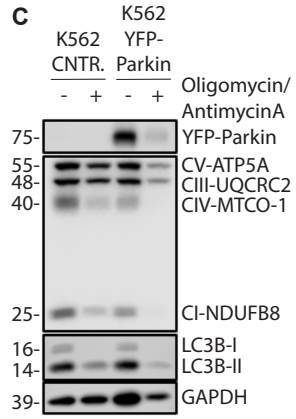
C
K562 CNTR.
K562 YFP-Parkin
Oligomycin/ AntimycinA
YFP-Parkin
CV-ATP5A
CIII-UQCRC2
CIV-MTCO-1
CI-NDUFB8
LC3B-I
LC3B-II
GAPDH

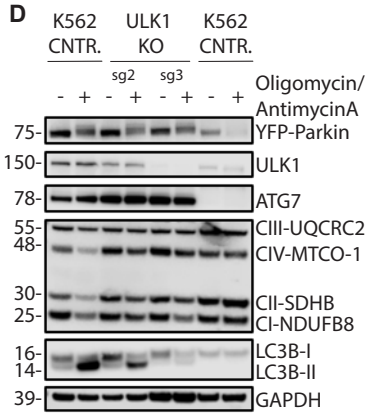
D
K562 CNTR.
ULK1 KO
K562 CNTR.
sg2
sg3
Oligomycin/ AntimycinA
YFP-Parkin
ULK1
ATG7
CIII-UQCRC2
CIV-MTCO-1
CII-SDHB
CI-NDUFB8
LC3B-I
LC3B-II
GAPDH

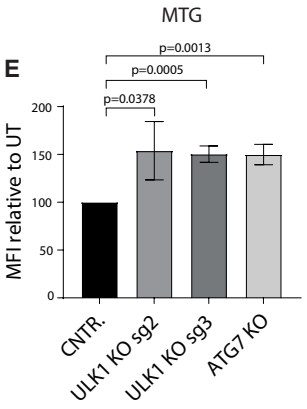
E
MTG
MFI relative to UT
p=0.0013
p=0.0005
p=0.0378
CNTR.
ULK1 KO sg2
ULK1 KO sg3
ATG7 KO

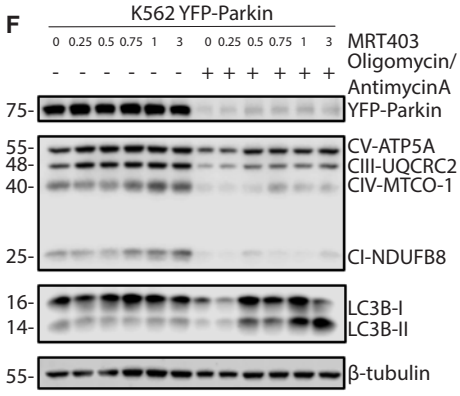
F
K562 YFP-Parkin
MRT403
Oligomycin/ AntimycinA
YFP-Parkin
CV-ATP5A
CIII-UQCRC2
CIV-MTCO-1
CI-NDUFB8
LC3B-I
LC3B-II
β-tubulin

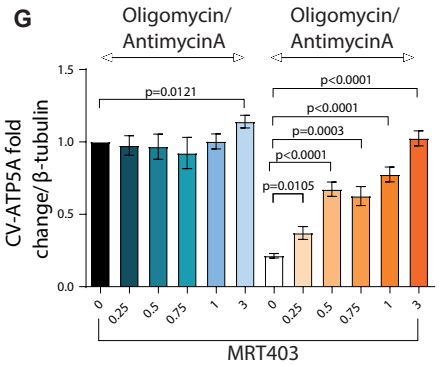
G
Oligomycin/ AntimycinA
Oligomycin/ AntimycinA
CV-ATP5A fold change/β-tubulin
p=0.0121
p<0.0001
p<0.0001
p=0.0003
p<0.0001
p=0.0105
MRT403

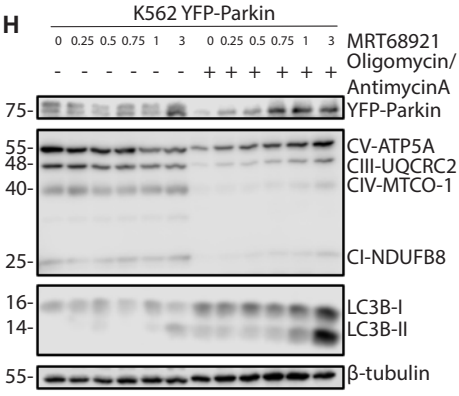
H
K562 YFP-Parkin
MRT68921
Oligomycin/ AntimycinA
YFP-Parkin
CV-ATP5A
CIII-UQCRC2
CIV-MTCO-1
CI-NDUFB8
LC3B-I
LC3B-II
β-tubulin

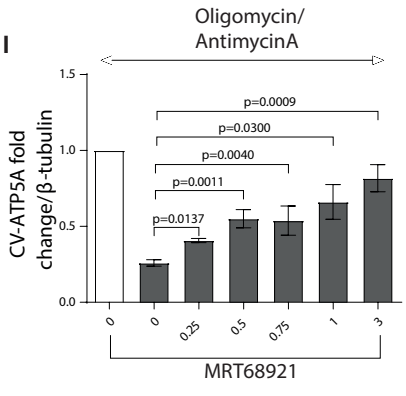
I
Oligomycin/ AntimycinA
CV-ATP5A fold change/β-tubulin
p=0.0009
p=0.0300
p=0.0040
p=0.0011
p=0.0137
MRT68921

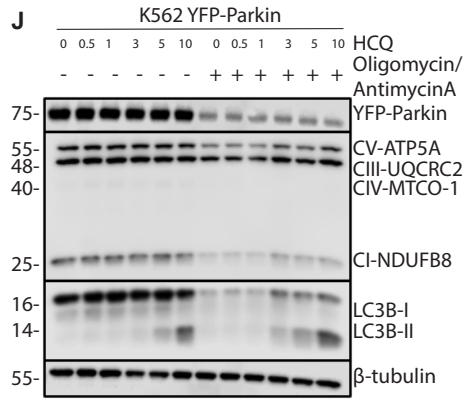
J
K562 YFP-Parkin
HCQ
Oligomycin/ AntimycinA
YFP-Parkin
CV-ATP5A
CIII-UQCRC2
CIV-MTCO-1
CI-NDUFB8
LC3B-I
LC3B-II
β-tubulin

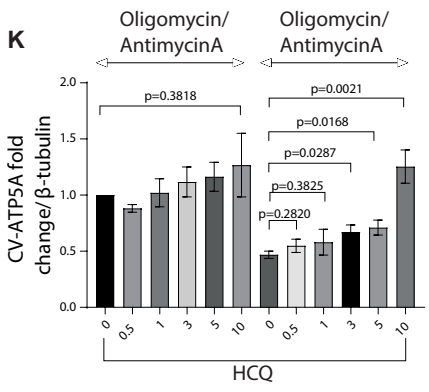
K
Oligomycin/ AntimycinA
Oligomycin/ AntimycinA
CV-ATP5A fold change/β-tubulin
p=0.3818
p=0.0021
p=0.0168
p=0.0287
p=0.3825
p=0.2820
HCQ

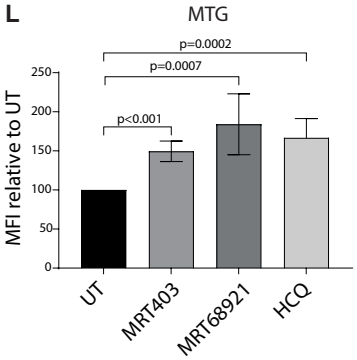
L
MTG
MFI relative to UT
p=0.0002
p=0.0007
p<0.001
UT
MRT403
MRT68921
HCQ

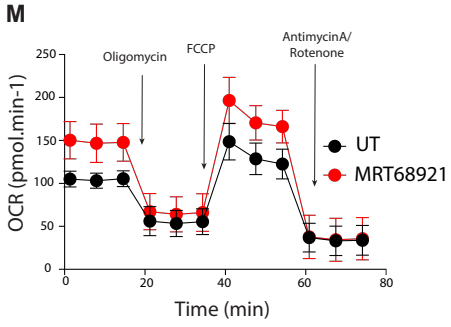
M
Oligomycin
FCCP
AntimycinA/ Rotenone
OCR (pmol.min-1)
UT
MRT68921
Time (min)

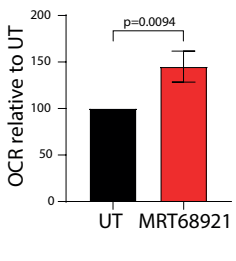
OCR relative to UT
p=0.0094
UT
MRT68921

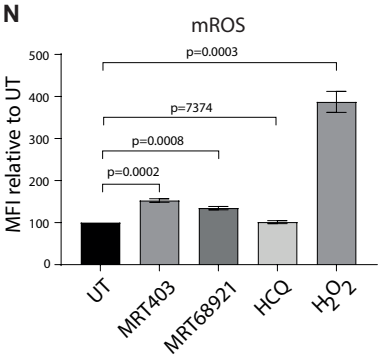
N
mROS
MFI relative to UT
p=0.0003
p=7374
p=0.0008
p=0.0002
UT
MRT403
MRT68921
HCQ
H2O2

Figure S2. Inhibition of ULK1 Induces Mitochondrial Respiration and Oxidative Stress

(**A**) Percent activity inhibition of 80 recombinant kinases using 1µM MRT68921 or 1µM MRT403. (**B**) Western blot showing protein expression and phosphorylation in KCL22 cells exposed to 2µM nilotinib, 3µM MRT403, 1µM MRT68921 and the combination of either 3µM MRT403 or 1µM MRT68921 with 2µM nilotinib for 24h. (**C**) Western blot showing mitochondrial protein expression in control and YFP-Parkin expressing K562 cells exposed to 1nM of antimycinA and 1nM oligomycin for 24h. (**D**) Representative western blot showing mitochondrial protein levels following 12h exposure to 1nM of antimycinA and 1nM of oligomycin in control, ULK1 and ATG7 deficient cells. (**E**) Measurements of mitochondrial mass using mitotracker green (MTG) fluorescent dye in ULK1 or ATG7 KO K562 cells (n=3). Mean ± S.D. P-values were calculated using unpaired Student's T-test. (**F-H-J**) Representative western blot showing mitochondrial protein expression in K562 YFP-Parkin cells exposed to 1nM of antimycinA, 1nM of oligomycin and increasing concentration (0-3µM) of MRT403 or (0-3µM) MRT68921 or (0-10µM) HCQ for 24h. (**G-I-K**) Relative CV-ATP5A change following treatment with increasing concentration (0-3µM) of MRT403 (n=5) or MRT68921 or HCQ (n=4). Mean ± S.E.M. P-values were calculated using unpaired Student's T-test. (**L**) Measurements of mitochondrial mass using mitotracker green (MTG) fluorescent dye following treatment using 3µM MRT403, 1µM MRT68921 or 3µM HCQ for 3 days (n=3). Mean ± S.D. P-values were calculated using unpaired Student's T-test. (**M**) Representative OCR profile in $CD34^+$ CML cells exposed to MRT68921 for 24h**.** Graphs showing relative basal OCR (n=3). Mean ± S.D. P-values were calculated using unpaired Student's T-test. (**N**) Measurements of mitochondrial ROS following exposure to 3µM MRT403, 1µM MRT68921 or 3µM HCQ (n=3). Mean ± S.D. P-values were calculated using unpaired Student's T-test.

Fig. S3

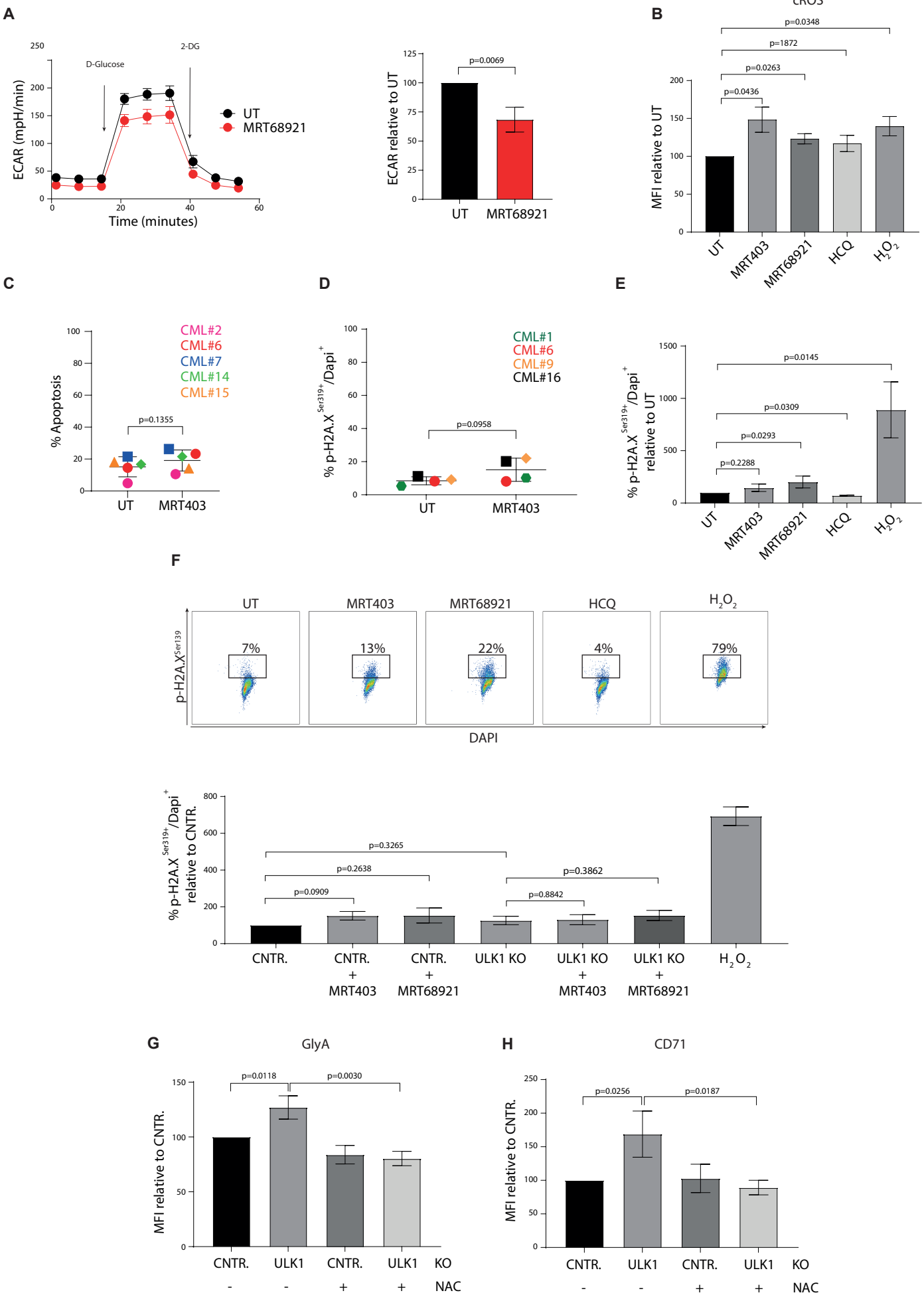
A
ECAR (mpH/min)
Time (minutes)
D-Glucose
2-DG
UT
MRT68921
ECAR relative to UT
p=0.0069
B
cROS
MFI relative to UT
p=0.0348
p=1872
p=0.0263
p=0.0436
UT
MRT403
MRT68921
HCQ
H2O2
C
% Apoptosis
CML#2
CML#6
CML#7
CML#14
CML#15
p=0.1355
D
% p-H2A.X Ser319+ /Dapi+
CML#1
CML#6
CML#9
CML#16
p=0.0958
E
% p-H2A.X Ser319+ /Dapi+ relative to UT
p=0.0145
p=0.0309
p=0.0293
p=0.2288
F
p-H2A.X Ser139
DAPI
7%
13%
22%
4%
79%
% p-H2A.X Ser319+ /Dapi+ relative to CNTR.
p=0.3265
p=0.2638
p=0.0909
p=0.3862
p=0.8842
CNTR.
CNTR. + MRT403
CNTR. + MRT68921
ULK1 KO
ULK1 KO + MRT403
ULK1 KO + MRT68921
G
GlyA
MFI relative to CNTR.
p=0.0118
p=0.0030
ULK1
KO
NAC
H
CD71
p=0.0256
p=0.0187

Figure S3. MRT403-Mediated ULK1 Inhibition Promotes Loss of Quiescence and ROS-Dependent Differentiation

(**A**) Representative ECAR profile in $CD34^+$ CML cells exposed to 1µM MRT68921 for 3 days. Graphs showing relative basal ECAR (n=3). Mean ± S.E.M. P-values were calculated using unpaired Student's T-test. (**B**) Measurements of cellular ROS following exposure to 3µM MRT403, 1µM MRT68921 or 3µM HCQ (n=3). Mean ± S.D. P-values were calculated using unpaired Student's T-test. (**C**) Measurements of apoptosis in $CD34^+$ CML following exposure to 3µM MRT403 for 3 days (n=5). Mean ± S.D. P-values were calculated using paired Student's T-test. (**D**) Measurements of DNA damage in $CD34^+$ CML following exposure to 3µM MRT403 for 3 days (n=4). Mean ± S.D. P-values were calculated using paired Student's T-test. (**E**) Representative flow cytometry plots and graph showing measurements of DNA damage in KCL22 following exposure to 3µM MRT403, 1µM MRT68921 and 3µM HCQ for 3 days and H_2O_2 for 1h (n=3). Mean ± S.D. P-values were calculated using paired Student's T-test. (**F**) Measurement of DNA damage in KCL22 control and ULK1 KO following exposure to 3µM MRT403 and 1µM MRT68921 for 3 days and H_2O_2 for 1h (n=3). Mean ± S.D. P-values were calculated using paired Student's T-test. (**G-H**) Relative MFI for GlyA or CD71 expression in ULK1 KO CML cells. Differentiation was reverted using NAC (100mM). Mean ± S.D. P-values were calculated using unpaired Student's T-test.

Fig. S4

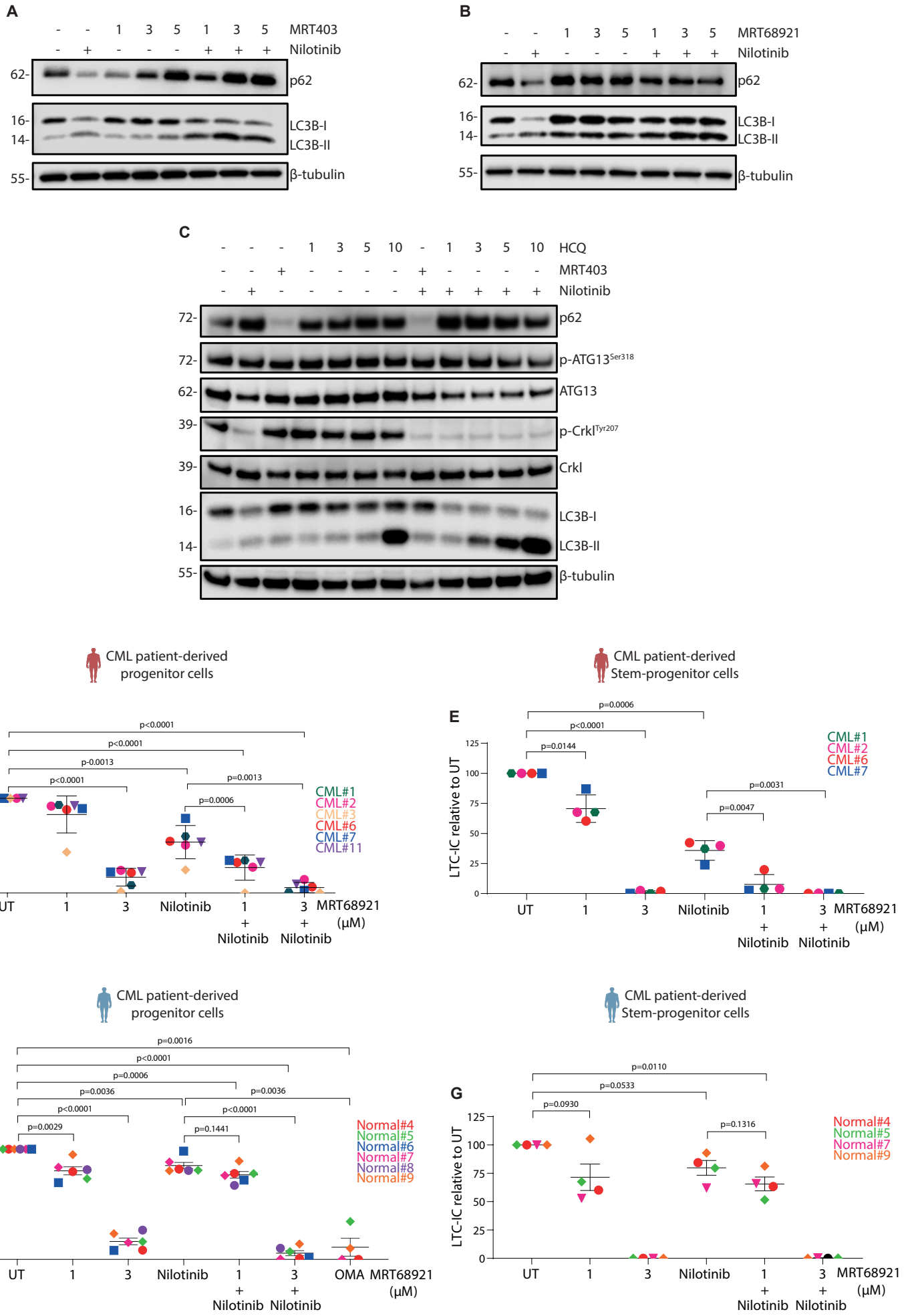
A
MRT403
Nilotinib
62-
p62
16-
14-
LC3B-I
LC3B-II
55-
β-tubulin
B
MRT68921
Nilotinib
p62
LC3B-I
LC3B-II
β-tubulin
C
HCQ
MRT403
Nilotinib
72-
p62
p-ATG13Ser318
62-
ATG13
39-
p-CrkITyr207
CrkI
LC3B-I
LC3B-II
β-tubulin
CML patient-derived progenitor cells
D
CFC relative to UT
CML#1
CML#2
CML#3
CML#6
CML#7
CML#11
UT
Nilotinib
MRT68921 (μM)
CML patient-derived Stem-progenitor cells
E
LTC-IC relative to UT
CML#1
CML#2
CML#6
CML#7
CML patient-derived progenitor cells
F
CFC relative to UT
Normal#4
Normal#5
Normal#6
Normal#7
Normal#8
Normal#9
OMA
CML patient-derived Stem-progenitor cells
G
LTC-IC relative to UT
Normal#4
Normal#5
Normal#7
Normal#9

Figure S4. MRT403 Treatment Inhibits TKI-Induced Autophagy and Targets CML LSCs

(**A-C**) Western blot showing autophagy protein expression exposed to increased concentration (0-5μM) of MRT403 or MRT68921 or (0-10μM) of HCQ for 24h. (**D**) Relative CFC following exposure of $CD34^+$ CML cells to 2 μM nilotinib, 1-3μM MRT68921 and the combination of nilotinib and MRT68921 for 3 days (n=6). (**E**) Relative LTC-IC following exposure of $CD34^+$ CML cells to 2μM nilotinib, 1-3μM MRT68921 and the combination of nilotinib and MRT68921 for 3 days (n=4). (**F**) Relative CFC following exposure of normal $CD34^+$ cells to 2 μM nilotinib, 1-3μM MRT68921, 100nM Omacetaxine and the combination of nilotinib and MRT68921 for 3 days (n=6). (**G**) Relative LTC-IC following exposure of normal $CD34^+$ cells to 2 μM nilotinib, 1-3μM MRT68921 and the combination of nilotinib and MRT68921 for 3 days (n=4). Mean ± S.D. or S.E.M. P-values were calculated using paired Student's T-test where appropirate.

Fig. S5

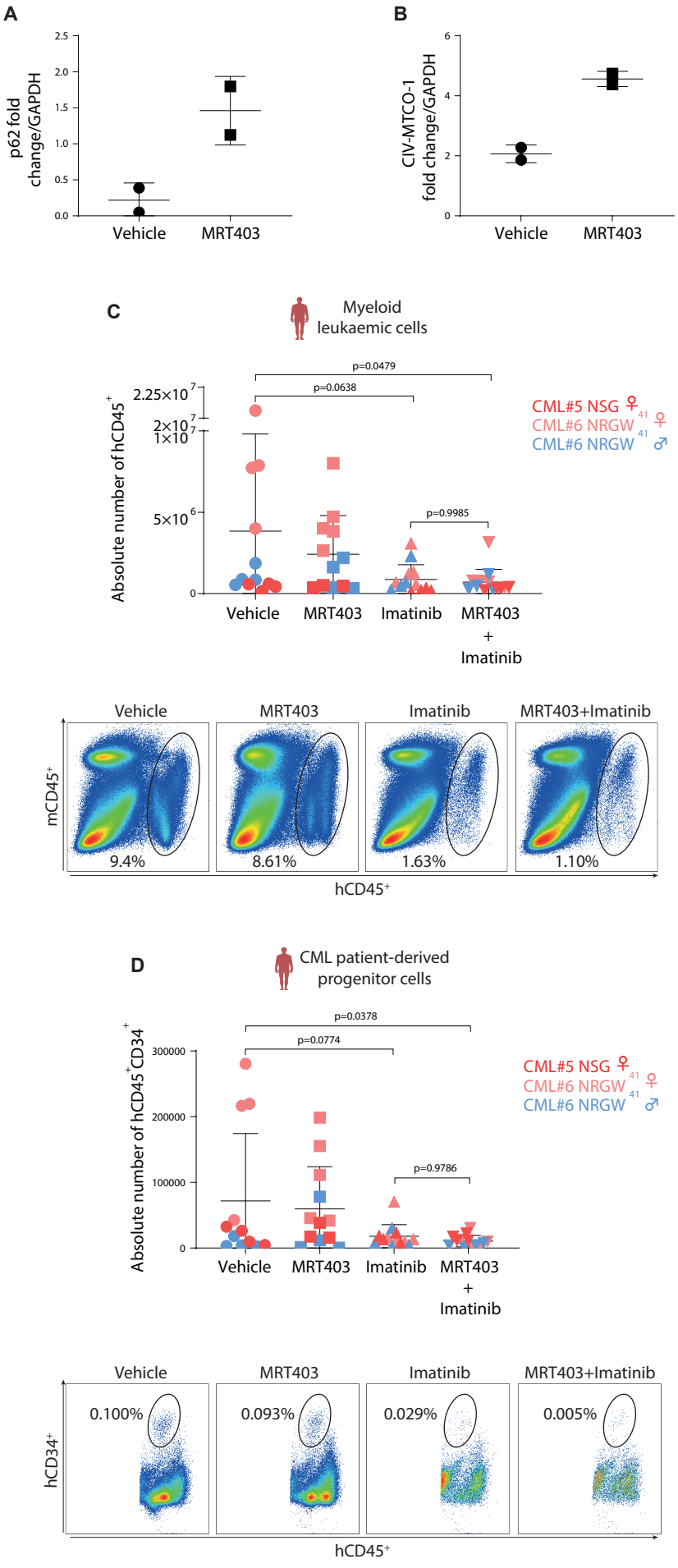
A
p62 fold change/GAPDH
2.5
2.0
1.5
1.0
0.5
0.0
Vehicle
MRT403
B
CIV-MTCO-1 fold change/GAPDH
6
4
2
0
Vehicle
MRT403
C
Myeloid leukaemic cells
p=0.0479
p=0.0638
p=0.9985
Absolute number of hCD45+
2.25×10^7
2×10^7
1×10^7
5×10^6
0
CML#5 NSG ♀41
CML#6 NRGW ♀41
CML#6 NRGW ♂41
Vehicle
MRT403
Imatinib
MRT403 + Imatinib
Vehicle
MRT403
Imatinib
MRT403+Imatinib
mCD45+
9.4%
8.61%
1.63%
1.10%
hCD45+
D
CML patient-derived progenitor cells
p=0.0378
p=0.0774
p=0.9786
Absolute number of hCD45+CD34+
300000
200000
100000
0
CML#5 NSG ♀41
CML#6 NRGW ♀41
CML#6 NRGW ♂41
Vehicle
MRT403
Imatinib
MRT403 + Imatinib
Vehicle
MRT403
Imatinib
MRT403+Imatinib
hCD34+
0.100%
0.093%
0.029%
0.005%
hCD45+

Figure S5. MRT403 Targets Human CML LSC Xenografts when Combined with TKI Treatment

(**A-B**) Fold change of p62 or ETC-CIV in human $CD45^+$ following 5 days in vivo treatment with MRT403. (**C**) Absolute number of transplanted human CD45 following in vivo treatment of female NSG, female/male $NRGW^{41}$ with MRT403 (40mg/kg; QD), imatinib (50mg/kg; BID) or the combination for 4 weeks. Mean ± S.D. P-values were calculated using one-way ANOVA and Dunnett's multiple comparisons test. (**D**) Absolute number of transplanted human $CD45^+CD34^+$ following in vivo treatment of female NSG, female/male $NRGW^{41}$ with MRT403 (40mg/kg; QD), imatinib (50mg/kg; BID) or the combination for 4 weeks. Mean ± S.D. P-values were calculated using one-way ANOVA and Dunnett's multiple comparisons test. Representative flow cytometry plots showing expression of human CD45 and human CD34 surface markers.

Fig. S6

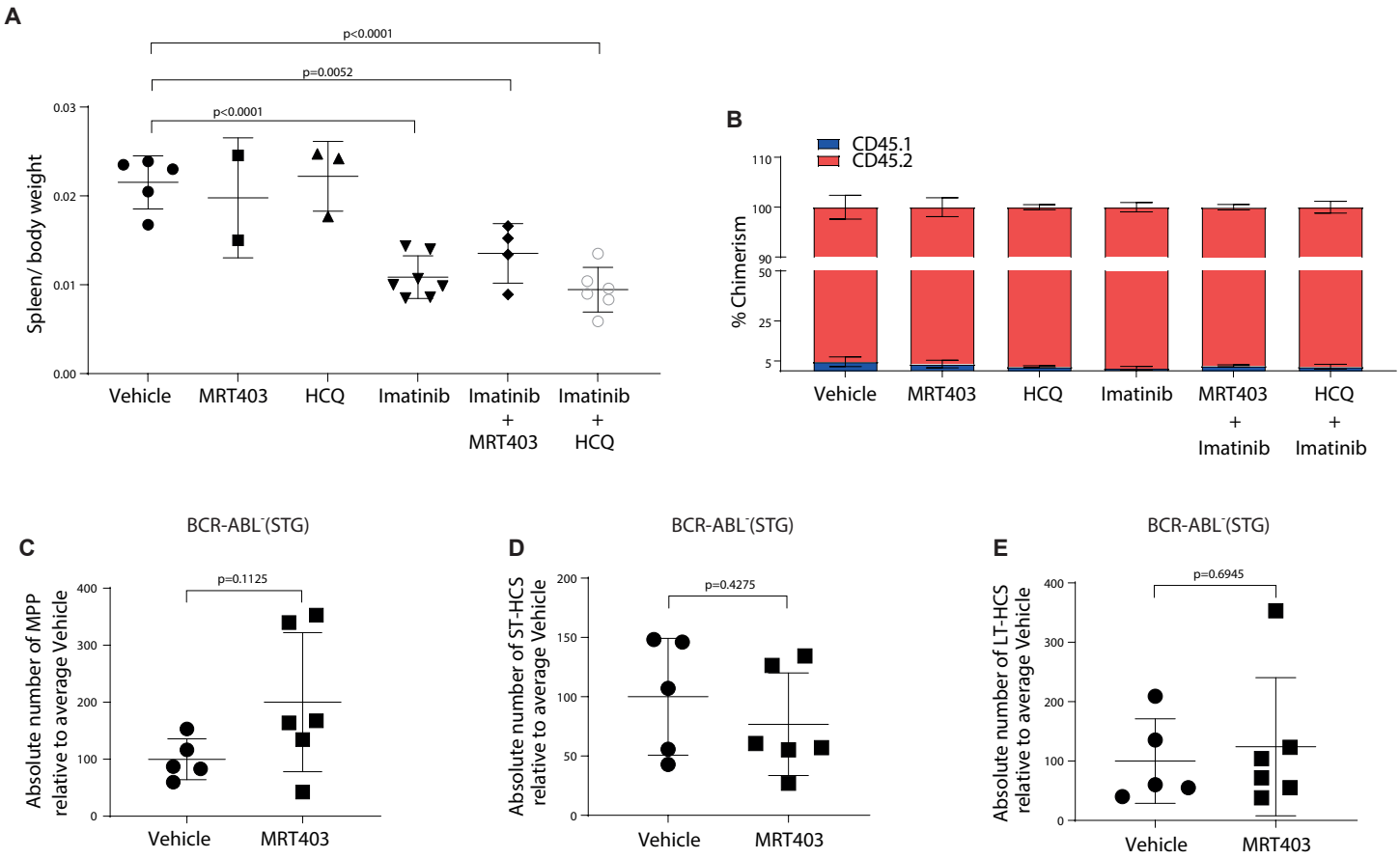
A
p<0.0001
p=0.0052
p<0.0001
Spleen/ body weight
0.03
0.02
0.01
0.00
Vehicle
MRT403
HCQ
Imatinib
Imatinib + MRT403
Imatinib + HCQ
B
CD45.1
CD45.2
% Chimerism
110
100
90
50
25
5
Vehicle
MRT403
HCQ
Imatinib
MRT403 + Imatinib
HCQ + Imatinib
C
BCR-ABL⁻(STG)
p=0.1125
Absolute number of MPP relative to average Vehicle
400
300
200
100
0
Vehicle
MRT403
D
BCR-ABL⁻(STG)
p=0.4275
Absolute number of ST-HCS relative to average Vehicle
200
150
100
50
0
Vehicle
MRT403
E
BCR-ABL⁻(STG)
p=0.6945
Absolute number of LT-HCS relative to average Vehicle
400
300
200
100
0
Vehicle
MRT403

Figure S6. MRT403 and TKI Combination Selectively Targets LSCs in an Inducible CML Model

(**A**) Graphical demonstration of spleen weight relative to body weight from each treatment arm with either MRT403 (40mg/kg; QD), imatinib (50mg/kg; BID) or the combination for 4 weeks. Mean ± S.D. P-values were calculated using paired Student's T-test. (**B**) BM CD45.1/CD45.2 primary transplant chimerism. Mean ± S.D. P-values were calculated using paired Student's T-test. (**C-E**) Absolute number of BM multipotent progenitor cells (MPPs), short-term (ST)-HSCs and LT-HSCs relative to average of vehicle treated mice. Mean ± S.D. P-values were calculated using unpaired Student's T-test.

Fig. S7

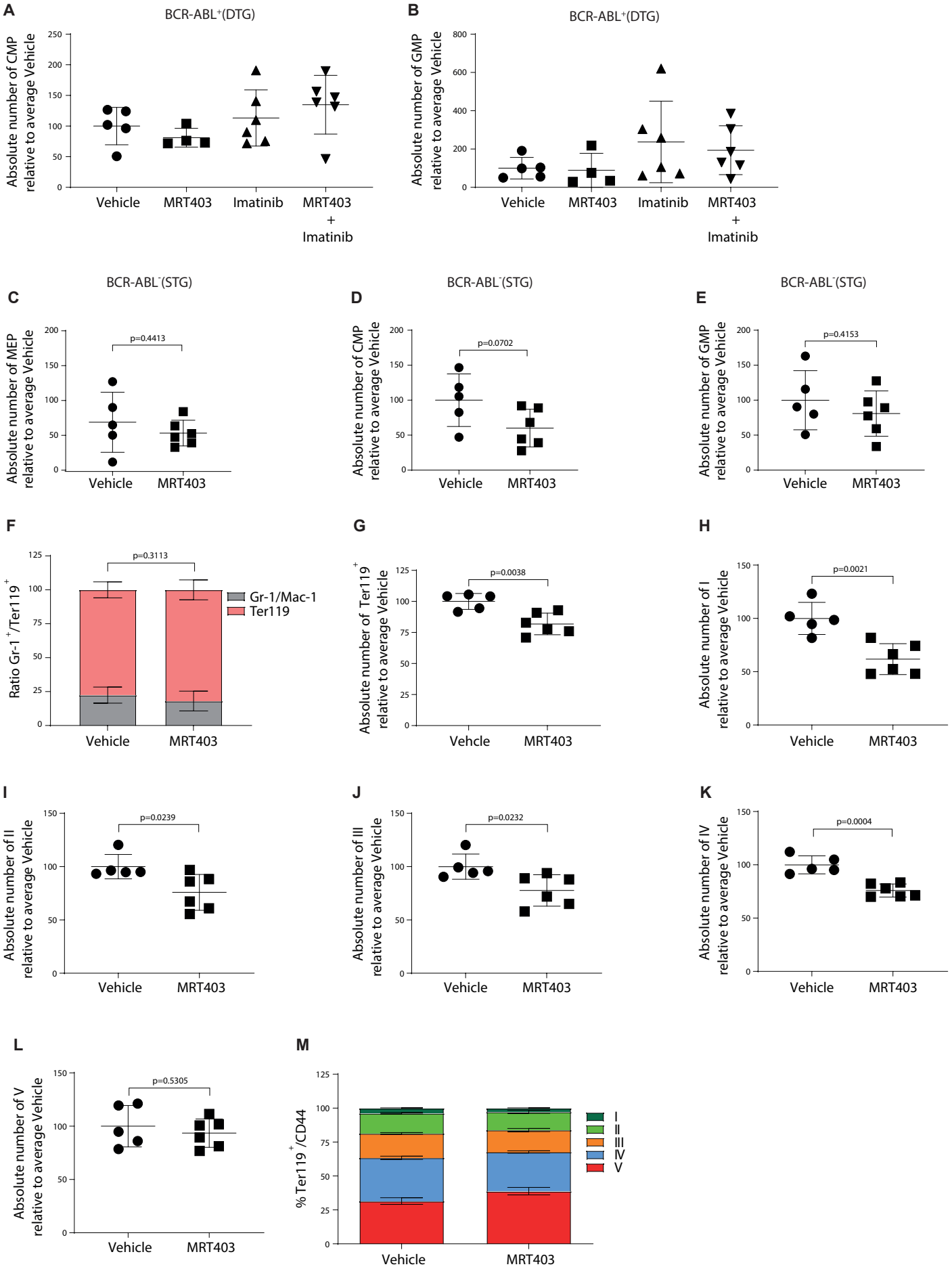
A
BCR-ABL+(DTG)
Absolute number of CMP relative to average Vehicle
Vehicle
MRT403
Imatinib
MRT403 + Imatinib
B
BCR-ABL+(DTG)
Absolute number of GMP relative to average Vehicle
C
BCR-ABL-(STG)
Absolute number of MEP relative to average Vehicle
p=0.4413
D
BCR-ABL-(STG)
Absolute number of CMP relative to average Vehicle
p=0.0702
E
BCR-ABL-(STG)
Absolute number of GMP relative to average Vehicle
p=0.4153
F
Ratio Gr-1+/Ter119+
p=0.3113
Gr-1/Mac-1
Ter119
G
Absolute number of Ter119+ relative to average Vehicle
p=0.0038
Vehcle
H
Absolute number of I relative to average Vehicle
p=0.0021
I
Absolute number of II relative to average Vehicle
p=0.0239
J
Absolute number of III relative to average Vehicle
p=0.0232
K
Absolute number of IV relative to average Vehicle
p=0.0004
L
Absolute number of V relative to average Vehicle
p=0.5305
M
% Ter119+/CD44
I
II
III
IV
V

Figure S7. Combination of MRT403 and TKI Treatment Restores Erythropoiesis

(**A-B**) Absolute number of BCR-ABL^{+} BM CMPs and GMP relative to average of vehicle treated leukaemic mice. (**C-E**) Absolute number of BCR-ABL^{-} BM CMPs, GMPs and MEPs relative to average of vehicle treated mice. (**F**) Ratio of BM Gr-1^{+}/Mac-1^{+} and Ter119^{+} cells from each treatment arm. (**G**) Absolute number of BM Ter119^{+} cells relative to average of vehicle treated mice. (**H-L**) Absolute number of BM pro-erythroblasts (region I), basophilic erythroblasts (region II), polychromatic erythroblasts (region III), orthochromatic erythroblasts/immature reticulocytes V and mature red blood cells (region V). Mean ± S.D. P-values were calculated using unpaired Student's T-test for all experiments previsions. (**M**) Ratio of separate erythroid populations (regions I-V) from each treatment arm.

Table S1

Primary sample	Gender	Age	TKI response	Additional clinical information
CML#1	Male	56	Responder	Imatinib intolerant; optimal response to dasatinib (in MR4.5)
CML#2	Male	58	No data available	
CML#3	Male	69	Non-responder	Failed imatinib, progression to blast phase on dasatinib.
CML#4	N/A	N/A	Responder	Suboptimal response (BCR-ABL 0.11% at 12 months, MMR achieved by 18 months).
CML#5	Male	46	Non-responder	CHR but no CCR on imatinib, no response to nilotinib nor dasatinib (referred for SCT)
CML#6	Female	63	Responder	Failed imatinib; MMR achieved on dasatinib.
CML#7	-	-	Responder	Optimal response (MR4 achieved on imatinib)
CML#8	Male	46	Responder	Failed imatinib; suboptimal response to bosutinib (in CCR, but not MMR)
CML#9	-	-	Responder	Optimal response (BCR-ABL 0.04% at 12 months)
CML#10	Female	52	Responder	Initially suboptimal response to imatinib, intolerant to dasatinib, now in MMR on imatinib; slow responder
CML#11	N/A	N/A	No data available	
CML#12	Male	68	Responder	Slow response (achieved CHR but not CCR on imatinib at 6 and 12 months).
CML#13	N/A	N/A	Responder	Failed imatinib (no CCR at 12 months), optimal response to dasatinib (in MMR)
CML#14	Male	40	Non-responder	Resistance to all TKIs (not in CCR, currently on ponatinib, possibly poor compliance)
CML#15	N/A	N/A	Responder	Imatinib intolerant; optimal response to nilotinib (in MR4.5)
CML#16	N/A	N/A	Responder	Optimal response to imatinib (BCR-ABL<10% at 3 months, <1% at 12 months, MMR at 18 months)

Responder: defined as <10% BCR-ABL (IS) at 3, 6 or 12 months.

Non-responder: Defined as >10% BCR-ABL (IS) at 12 months

Table S1: Table providing clinical information about individual CML samples used in the study.

Table S2

Kinase hit	MRT68921				MRT403			
	IC50 (nM)	SD	N	Fold selectivity	IC50 (nM)	SD	N	Fold selectivity
ULK1	7.6	2.8	6	-	1.6	0.6	2	-
ULK2	1	0.1	2	0.1	1.25	0.07	2	0.8
NUAK1	2.6	-	1	0.3	87.7	-	1	54.8
MARK3	3.4	0.6	2	0.4	299	-	1	186.9
TBK1	7.1	0.9	2	0.9	>3000	-	1	>1000
PKD1	19.5		1	2.6	6.3	-	1	3.9
JAK2	39.8	21.5	3	5.1	1430	115	3	893.8
AMPK	61.7	19	3	8	1300	405	4	812.5
CamKKbeta	234.4	-	1	30.8	203	-	1	126.9

Table S2: Table showing kinase hit *in vitro* IC50 using MRT68921 or MRT403.

Table S3

SAMPLE ID	MRT403 concentration	
	Plasma (ng/mL)	**µM**
Day 1 (5mg/kg) Vehicle	<LLOQ	<LLOQ
Day 1 (5mg/kg) MRT403	411	0.85
Day 1 (5mg/kg) MRT403	778	1.61
Day 5 (10mg/kg) Vehicle	<LLOQ	<LLOQ
Day 5 (10mg/kg) MRT403	1348	2.79
Day 5 (10mg/kg) MRT403	1711	3.54
Day 5 (40mg/kg) Vehicle	<LLOQ	<LLOQ
Day 5 (40mg/kg) MRT403	1093	2.26
Day 5 (40mg/kg) MRT403	1139	2.36

Table S3: Table showing MRT403 plasma concentration following *in vivo* dose escalation study where mice received 5, 10, and 40mg/kg dose for 5 days each dose. LLOQ = Below Limit of Quantification.